Development of a disposable and easy-to-fabricate PCR microfluidic device for DNA amplification

By

Hirad Mashouf

B.Sc., University of Tehran, Iran, 2020

A Thesis Submitted in Partial Fulfillment of the

Requirements for the Degree of

Master of Applied Science

in the Department of Mechanical Engineering

University of Victoria

Supervisory Committee

Development of a disposable and easy-to-fabricate PCR microfluidic device for DNA amplification

By

Hirad Mashouf

B.Sc., University of Tehran, Iran, 2020

Supervisory committee

Dr. Mina Hoorfar, Supervisor
Department of Mechanical Engineering

Dr. Mohsen Akbari, Departmental Member
Department of Mechanical Engineering,

Abstract

Polymerase chain reaction (PCR) is a technique in nucleic acid analysis which revolutionized molecular biology due to its numerous applications in medicine, biomedical devices, and forensics. PCR is used to amplify a considerable number of specific DNA target sequences from a minimal amount conducted by apparatus called thermal cyclers. The process involves repetitive heating and cooling the sample according to a specific protocol. Protocols usually consist of three steps: a denaturing step at 92–96°C, an annealing step at 52-58°C, and an extending step at 70-80°C. Microfluidic PCR devices suggest significant benefits over conventional thermal cyclers, such as smaller size, rapid heat transfer, portability, and lower sample consumption. However, most developed microfluidic chips require various external components to operate. They are also unsuitable for mass production due to their high cost and complex fabrication methods.

In this study, a disposable, low-cost, and easy-to-fabricate microfluidic PCR is developed. The device comprises a micromixer, reaction well, microheater, and temperature control system. Several methods have been implemented to reduce the chance of sample-to-sample cross-contamination. The designed control system is able to perform PCR at any temperature inside the ordinary working range of PCR protocols. The microheater is fabricated by patterning gold on a glass slide which has been modified through a series of experiments to provide temperature uniformity with ±1°C precision across a circular area that houses the PCR reaction chamber. The micromixer performance was analyzed at different flow rates and channel heights among several structures which culminated in final mixing efficiency of 94.17%. Finally, the reliability and repeatability of the microfluidic device were verified by amplifying λ DNA, where even the developed device outperformed conventional thermal cycler in specific protocols.

Table of Contents

List of Figures

List of Tables

Acknowledgements

I would like to express my gratitude to all my fellow lab mates for their help and support. I would like to express my gratitude to my supervisor, Dr. Mina Hoorfar, for her encouragement and enthusiasm in this study, and Nishat Tasnim for her assistance.

From University of British Columbia, I would like to thank Dr. Sepideh Pakpour for broadening my perspective of the biological sciences, and also, I acknowledge Chris Seib for his expertise in cleanroom.

Dedication

I would like to dedicate my work to the passengers of flight PS752. Also, to all the people who have brutally been killed in the past 43 years and the ones who are still fighting for free Iran.

Chapter 1: Introduction

1.1 What is PCR?

It is extremely unlikely to come across someone who has not heard the word PCR. The term has been all over the news since the COVID-19 pandemic started in 2019. COVID-19 PCR test is a molecular test known as the most reliable method to detect the disease for people with or without symptoms [1]. However, polymerase chain reaction (PCR) is not a novel technique; instead, it has been in practice for more than 25 years in a variety of contexts, including forensics analyses and medical and clinical diagnostics [2]–[7]. Kary Mullis, who won the Nobel Prize in 1993 for his contribution to the development of PCR, invented this method in 1983 [8].

The acronym PCR stands for the molecular biology technique known as Polymerase Chain Reaction, which is used to amplify a specific target DNA sequence. To put it more simply, this test aims to determine whether or not a certain gene is present in the sample. In contrast to more conventional approaches to DNA cloning and amplification, which frequently take several days to complete, PCR can be completed in just a few hours [9]–[11].

PCR consists of two parts: Polymerase and Chain Reaction, which means repeating a step a number of times. An enzyme known as a polymerase is responsible for producing lengthy chains of polymers or nucleic acids. All known forms of life rely on nucleic acids, which are biopolymers or big biomolecules. Nucleic acids are responsible for the storage and expression of genetic information. Nucleotides are the monomers from which DNA and RNA are constructed. Polynucleotides, like DNA and RNA, are formed when nucleotides bind together. Nucleic acid is a general term for both DNA and RNA [12].

In a nutshell, PCR is a way to quickly make millions or billions of copies of a specific DNA sample. This lets scientists take a tiny amount of DNA and make it into a large enough

amount to study in detail for molecular and even genetic analyses. Each PCR cycle usually consists of three steps [13], [14]. Figure 1 shows the result of one cycle in which a double-stranded DNA turns into two.

Denaturation is the first step in a PCR cycle. At this point in the process, a double strand of DNA is broken apart by subjecting it to a very high temperature. A denaturation step is required at the beginning of a PCR reaction before the three-step cycling procedure can begin. The initial denaturation phase typically takes place at 95°C (or in the range of 92°C - 96°C), but this value varies from polymerase to polymerase. The hydrogen bonds cannot be sustained at temperatures higher than 80°C, which is why double-stranded DNA denatures into single-stranded DNA at those temperatures. Initial denaturation can take up to 4 minutes to fully denature the DNA. However, extended incubation at this denaturation temperature could make polymerase inactive or cause damage to the DNA template. Typically, the denaturation stage is performed at the same temperature as the initial denaturation and takes only 10 - 40 seconds.

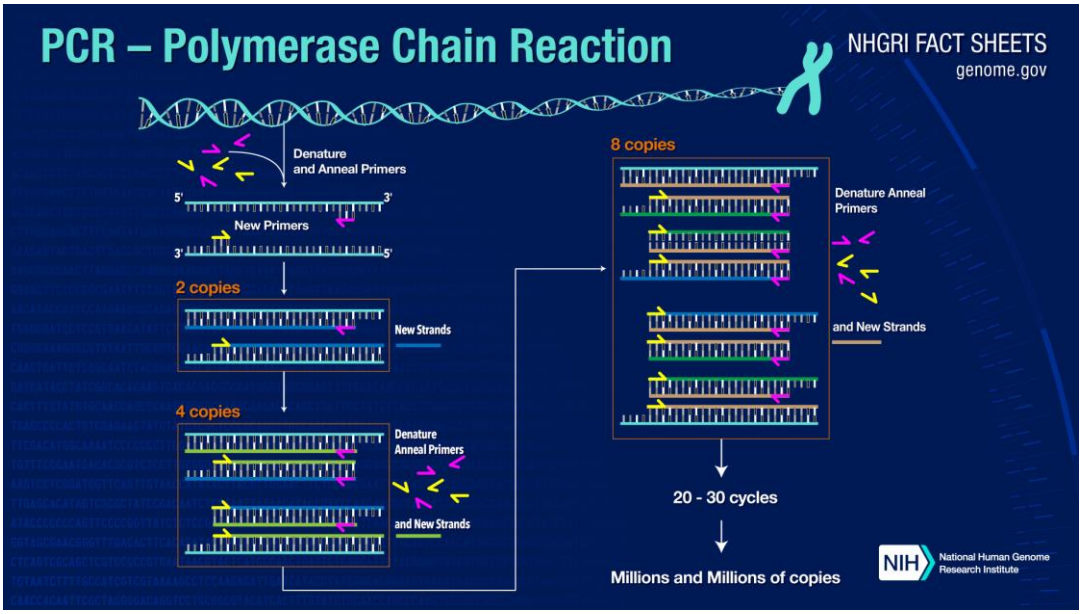

Figure 1 - Polymerase chain reaction (PCR) steps. Courtesy: National Human Genome Research Institute [15]

The subsequent step in PCR is annealing or hybridization. At this stage, primers bind to the denatured DNA strands, where they recognize a matching sequence. Primers are single-stranded sequences that are relatively short. Primers are typically between 10 and 30 nucleotides in length to ensure efficient hybridization with the target sequences in the matrix DNA. During annealing, the sample is cooled to a temperature of around 55°C. When the temperature is lowered, the hydrogen bonds reform, and the complementary strands hybridize with one another. The temperature and primer pair combinations must first be optimized before this may be done properly. The temperature during the annealing process ranges from 52°C to 58°C, and the process lasts for 15 to 60 seconds. Primer annealing efficiency suffers at high annealing temperatures, whereas non-specific template binding is possible at low annealing temperatures. It should be noted that primers are chemically generated, and there are many of them in the test environment, so there is a reasonable probability that they will bind with target DNA if being used.

The final phase of a cycle, known as extension or elongation, takes place at a temperature of about 72°C. The polymerase enzyme becomes active at this stage. This stage allows for optimal polymerase activity, which results in exponential amplification of the template strand by binding nucleotides to the annealed primer. Typically, the elongation process takes around one minute at 70°C - 80°C. As the temperature rises, the polymerase will begin to increase its activity and add nucleotides. The polymerase enzyme is most active and stable at these temperatures. In the same way that it is recommended to carry out an initial denaturation at the beginning of thermal cycling, it is likely that there will be one final extension period of five minutes at the end of thermal cycling.

In theory, the amount of DNA that was present in the cycle before will increase by a factor of two over each cycle. Creating a sufficient amount of DNA for analysis requires 20 - 40 cycles. Thermocyclers are the machines used for this procedure. Gel electrophoresis is typically used to

evaluate PCR reaction outcomes. Gel electrophoresis is a method that separates DNA fragments by size by pulling them through a gel matrix at the speed of an electric current. To determine the size of the fragments in the PCR sample, a standard, or DNA ladder, is frequently used. If the gel is stained with a loading dye, a band of DNA fragments of the same length can be observed by eye on the gel. Since DNA is so small, a DNA band containing the target DNA must have many copies of it to be visible to the naked eye.

1.2 Microfluidic PCR devices

The apparatus commonly utilized in laboratories to carry out PCR reactions is known as a conventional thermocycler. An enclosure is provided in these devices to deposit reaction tubes containing the PCR mixture. Peltier elements are typically used in the heating block of thermal cyclers to perform repetitive temperature cycles while the machine lets the user program the length and order of the cycles of temperature steps. Regular PCR machines must heat and cool not only the PCR mixture but the entire block and chambers. Because of the substantial thermal mass, the procedure would be time-consuming and energy-intensive. In addition, the sample preparation and post-PCR analysis need to be done off-line, and large quantities of expensive reagents are required [16].

Miniaturization is a new trend in the multidisciplinary study of analytical chemistry and the life sciences. The analytical tools and equipment used in laboratories today are more advanced, user-friendly, and compact than ever. This trend toward making things smaller also applies to the handling and analyzing of fluids. Microfluidics can be applied to a wide variety of applications, including cell detection, DNA sequencing, and sample pretreatment and analysis. Because of its potential and advantages, the usage of microfluidics in several applications is expanding at a rapid

rate: Including its high throughput, minimal sample and reagent volumes, autonomous operation, compact size, reduced time and energy consumption, and low cost [17]–[19].

When the idea of a lab-on-a-chip was introduced to make use of microfluidics in the field of biomedicine and chemistry, the development of microfluidic PCR equipment began. These devices have a number of benefits, including a high surface to volume ratio, a reduction in the quantity of reactants consumed, high controllability, and portability, all of which make them suitable for detection in the field. The PCR mixture will be subjected to more uniform temperatures throughout the PCR process, which will improve results, and the thermal cycling time will be decreased due to the rapid heat transfer to the sample mixture [20], [21].

1.2.1 Time domain and space domain PCR

Microfluidic PCR devices can be categorized into two groups: time domain PCR and space domain PCR. In time domain PCR, samples are injected and kept still in a reaction chamber. Active heating and cooling is used to continuously adjust the temperature of the chip [22]–[24]. Time domain PCRs are also referred to as well-based designs. Conversely, the sample is circulated through various predetermined temperature zones in space domain PCR [25]–[27]. The number of cycles and duration of the PCR heat stages are determined by the chip's design. During the course of a space domain PCR operation, the sample must be transported along the channel. Thus, they are also known by the term continuous-flow PCR [28], [29].

There are three subgroups for space domain PCR chips: closed-loop, oscillatory, and fixed-loop devices. The sample is transported around a fixed circuit in closed-loop PCR chips. In oscillatory systems, the sample is shuttled back and forth between chambers maintained at various temperatures. This causes the temperature of the sample to change continuously. In both designs,

the number of thermal cycles can be flexible, but in a fixed-loop system, the number of cycles must be chosen at the fabrication stage [30].

The first fixed-loop continuous-flow PCR was developed in 1998 [25]. Samples were made to move through a microfluidic channel while repeatedly passing through three temperature zones required for PCR. Copper blocks were used to maintain the protocol temperatures of 95°C, 77°C, and 60°C. In under 90 seconds, 10 μL sample could undergo 20 cycles of PCR.

Sun et al. [26] developed a closed-loop microchip for PCR with a circular channel that worked with ferrofluid. The PCR mixture is propelled across the three temperature zones by a small ferrofluid plug comprised of magnetic particles in a liquid carrier and guided along the circular microchannel by an external magnet. The external magnet's rotational speed determined each PCR cycle's duration. Altering the microchip arrangement's geometry also allows selecting various times for each of the three temperature zones.

Frey et al. [27] reported an oscillating-flow mechanism in which a single actuator, which was accomplished with the help of a pneumatic pump, deflected pumping membranes. Because of this, the sample was forced to pass through three different temperature zones. The capability of the devices to establish numerous channels in parallel to carry out PCR amplification at the same time is an appealing aspect of the products.

Time domain PCRs showed great potential for target DNA/RNA amplification and suggested satisfactory performance in integrated devices as well [22], [23], [31], [32]. A PCR microfluidic chip was developed by Cui et al. [24] and verified by amplifying β-actin gene DNA fragment. Their system consisted of a reusable heater and a disposable PCR chamber. A microsystem that could determine sex was reported by Lagally et al. [33]. The microfluidic chip was able to show PCR results in less than 15 minutes from human genomic DNA. Liu et al. [34]

fabricated a microfluidic chip that successfully conducted DNA amplification. The integrated device involved micropumps and microheater arrays. Jie et al. [35] presented a portable device for PCR amplification with end-point detection. They successfully performed nucleic acid amplification by powering the device with a 24V Li-ion battery. Wang et al. [36] detected four different DNA fragments of HIV-1 by conducting PCR on a microfluidic system. They included several micropumps and microvalves in their device, and after each process, the whole chip was washed with a washing buffer.

Many other on-chip PCR designs have also been reported in the literature, such as digital PCR and centrifugal devices [37]–[39]. These devices are whether hard to fabricate or require expensive equipment to operate. Fixed-loop space domain PCRs are not flexible in terms of cycle number. Other continuous-flow PCR designs require a source to transport the PCR mixture through the whole process.

1.3 Objectives

The work in this study is focused on time domain PCR. A vast majority of proposed PCR chips in this area have complex designs, require external equipment, and embrace various components. Thus, they are not a suitable option for mass production and point-of-care devices. The target is to design, fabricate, and test a microfluidic device for PCR reaction, which is cost-efficient in fabrication and operation. The proposed microfluidic device consists of three main parts: a micromixer, a reaction well, and a microheater. Each of these parts is studied separately and characterized to perform efficiently in terms of temperature uniformity, power consumption, size, and cost. The final integrated device has to be compact, disposable, low-cost, and easy to fabricate and operate. The Objective is to conduct PCR amplification on lambda (λ) phage bacterial virus which is a well characterized and readily available viral DNA.

Chapter 2: Reaction chamber and sample preparation

2.1 Design considerations

Micro reaction chamber is where PCR amplification takes place. PCR reagents are sensitive to contamination and easily degrade. Polydimethylsiloxane (PDMS) is one of the materials commonly used for the fabrication of reaction chambers. It is a well-known biocompatible material for biological applications. PDMS has good light permeability, adheres firmly to flat surfaces, and is suitable for mass production [2], [24], [40].

As discussed in the previous chapter, in continuous-flow PCR, the reaction occurs inside the channels. The channels acting as reaction chambers can be of any shape (serpentine, circular, etc.) depending on the position of thermal zones and thermal cycling mechanism. In contrast, time-domain PCRs have specific chambers for PCR reactions.

Simple reaction chambers are commonly used in biomedical applications such as PCR and cell detection [24], [41]. Reaction chambers are made in cylindrical shapes, referred to as reaction wells. Oblath et al. [42] conducted real-time polymerase chain reaction amplification of Streptococcus mutans from saliva samples. They used seven wells made of PDMS as reaction chambers. Using CNC machining and PDMS casting, Wang et al. [36] manufactured a microfluidic system that could detect DNA fragments of HIV-1 by conducting PCR inside four reaction wells. Lien et al. [43] fabricated an integrated microreverse transcription polymerase chain reaction system that could successfully detect two different types of viruses, Dengue virus serotype 2 and enterovirus 71, by completing PCR inside a reaction well.

In a few studies, a special chamber named Gene Frame® is employed [44]. The advantages of these ready-to-purchase chambers are that they do not inhibit PCR reactions and can withstand temperatures up to 97°C. However, their price prevents us from using them in our device.

This chapter begins with analyzing several reaction chamber structures. These structures are inspired by common reaction chambers in literature. However, it is tried to design a chamber with low-cost fabrication and convenient integration with other parts. Then, the reagents needed for PCR and their volumes are reported in detail. Finally, the PCR protocol is selected.

2.2 Reaction chambers

Reaction chambers are usually bonded on top of microheaters in lab-on-a-chip PCR devices. In our device, the reaction chamber is also located on top of the heater. The thermocycler characteristics will be discussed in the next chapter. First, two preliminary designs for reaction chambers are briefly discussed.

2.2.1 Simple rectangular chamber

The first design used for the reaction chamber was simple rectangular microchambers. Fabrication of these chambers was straightforward. The capacity of these chambers can be easily modified by changing the dimensions or height of the fabricated mold. These chambers were created by soft photolithography.

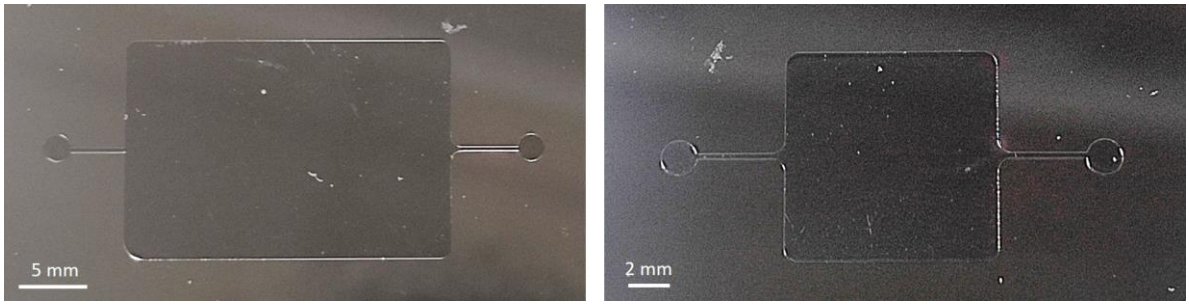

Figure 2 – Simple rectangular PCR chambers

Figure 2 shows silicon molds of two rectangular chambers of different capacities fabricated by photolithography. These chambers were not an appropriate option for our application. First, a large amount of liquid could not be retrieved from the chamber, which complicates post-PCR and

may even affect the result of amplification. Second, as the temperature rises, the pressure inside the chamber increases, which in turn, either damages the bonding or pushes out the samples inside the chamber.

2.2.2 Serpentine reaction chamber

Serpentine PCR chambers were designed next by getting inspired by space domain PCR channels. This design did not have the disadvantage of complex sample retrieving. The serpentine channels were also made by soft photolithography in different sizes to have various capacities.

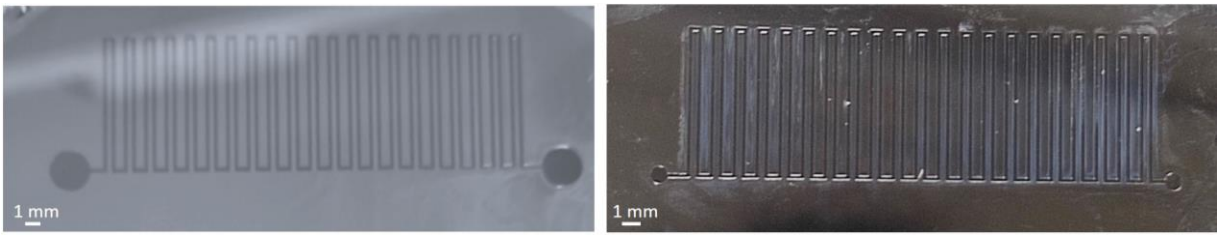

Figure 3 - Serpentine PCR chambers

Figure 3 shows the silicon molds of serpentine reaction chambers. Although fluid handling was easier in serpentine channels, it performed poorly during experiments.

Images in Figure 4a are captured in a time period of one minute. The chamber is bonded to a microscope glass slide and heated at 90°C by a hot plate. The water inside the channels was also dyed for better illustration. The formation of bubbles inside the chamber pushed the fluid out of the chambers rapidly, which is not favorable due to sample loss. Several approaches were implemented to solve this issue, such as increasing pressure from both sides or injecting mineral oil. Bubble formation was reduced, but the issue was not resolved entirely for successful PCR amplification. Other factors, such as non-uniform temperature distribution and inaccurate temperature sensing, might have also been the reason. Moreover, high pressure inside the channels to prevent bubble formation sometimes leads to bonding damage and sample leakage.

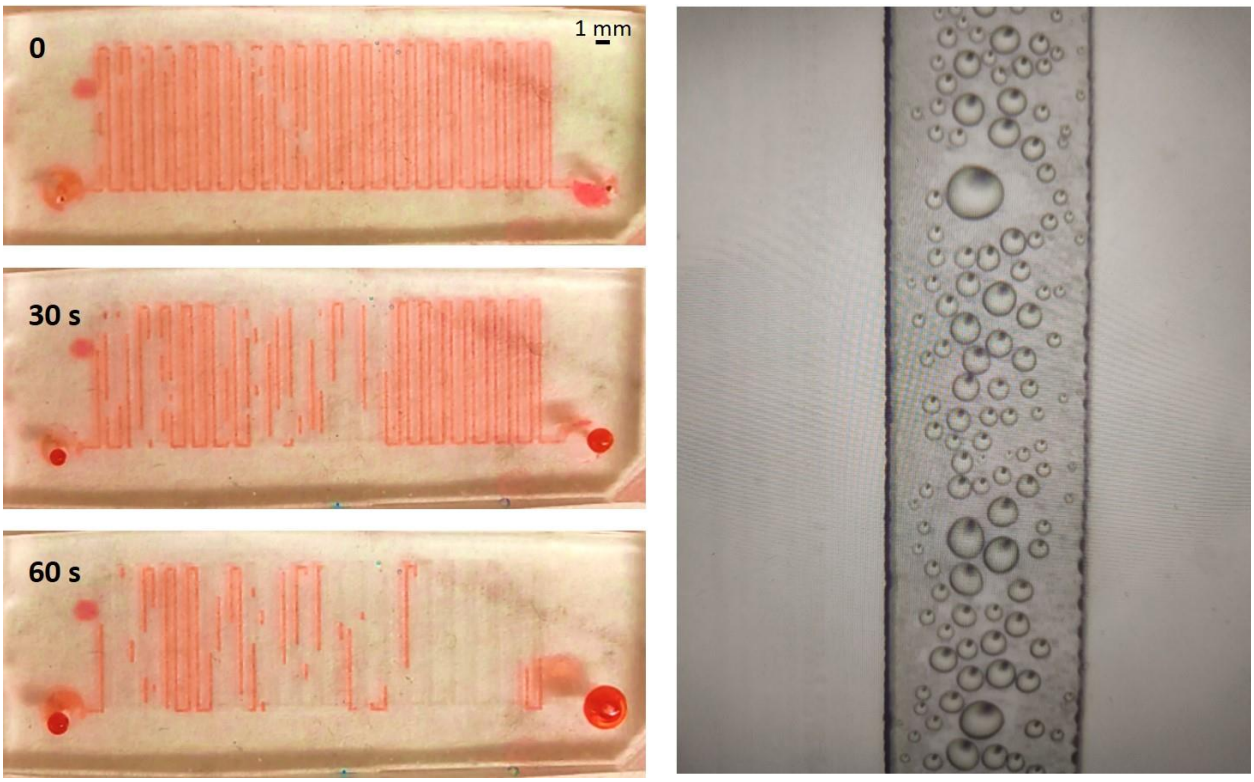

Figure 4 – Bubble formation inside serpentine PCR chambers. (a) fabricated chamber, and (b) Channels under the microscope

2.2.3 Reaction well

As reaction chambers did not provide satisfactory results, we decided to use reaction well. Reaction wells can be produced pretty easily. The simplest way is to punch a hole inside a block of PDMS, as shown in Figure 5.

Reaction wells present considerable advantages over reaction chambers for our application: First, their production does not need complex soft photolithography since PDMS blocks can be made with simple molds. Second, they can be manufactured in very compact structures with high capacities. As a result, they can be bonded to substrates other than the microheater, such as coverslips. This is not only beneficial in reducing the size of the whole device but also makes the microheater section reusable. Sensing and monitoring the mixture's temperature is more accurate

in PCR wells. Moreover, the amplified sample can be readily retrieved for post-PCR analysis. Integration of reaction well with other parts of the device is also more convenient. By making use of reaction wells, we eliminated the requirement for employing microvalves and micropumps, which is exceptionally advantageous and will be covered in further detail in subsequent chapters.

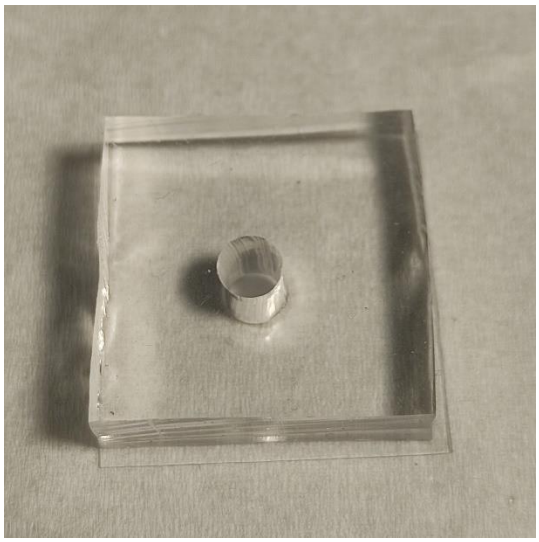

Figure 5 – Simple PDMS reaction well bonded on a coverslip

2.3 Fabrication

The steps for fabricating reaction wells are as follows: 10:1 weight ratio of PDMS pre-polymer and curing agent (SYLGARD™ 184, Dow Inc., MI, USA) was mixed. The mixture was poured into a mold and degassed for 5 minutes, followed by baking for 2 hours at 80°C in the oven to create PDMS sheets. These sheets with a thickness of 3 mm were then cut down into small blocks of 2×1.5 cm. Biopsy punches were used to make holes throughout the block to form the reaction well.

The size of the biopsy punch depends on the diameter of the well. Uniform temperature distribution inside the reaction well is crucial for high-quality PCR reaction. The temperature uniformity analysis is conducted, and the results are provided in the microheater chapter.

Temperature profiles for well diameters in the range of 3.5 mm and 5.5 mm are studied, and the appropriate size is chosen.

Evaporation and the development of bubbles were the most irritating occurrences that disrupted thermocycling while the experiments were conducted. We implemented several methods to prevent evaporation as much as possible. These methods included sealing the reaction well, covering it with mineral oil, heating from the top, etc.

The tests were conducted for 10 minutes at 95°C, implementing the mentioned solutions. Evaporation loss while not using any of the methods was more than 70 percent. We found that covering the sample with mineral oil would be the best option. Covering a sample of 20 µL with 10 µL of mineral oil demonstrated around 7% sample loss on average. Definitely, using more oil would decrease the sample loss due to evaporation, but the result from 10 µL mineral oil was sufficient.

2.4 Sample preparation

The PCR reactants were purchased from Integrated DNA technologies. The PCR master mix consists of 2 µL Deoxynucleoside triphosphate (dNTP), 2µL 10X PCR buffer, 1 µL MgCl2, 10.8 µL nuclease-free water, and 0.4 µL Taq gold (AmpliTaq Gold™ DNA Polymerase). The forward and reverse primers used were 5'- ATG CCA CGT AAG CGA AAC A -3', and 5'- GCA TAA ACG AAG CAG TCG AGT -3', respectively, each with 0.4 µL volume. The master mix (17 µL) was prepared inside a tube and then transferred to the disposable PCR chip to be mixed with 3 µL of 100-fold diluted λ-phage DNA inside the micromixer.

Upon PCR completion, 10 µL of the amplified product was taken out by pipetting and mixed with 2 µL of loading dye to be analyzed by gel electrophoresis in a 2% agarose gel

Invitrogen. The resulting DNA fragments size was measured by GeneRuler 100 bp DNA Ladder (SM0241, Thermo Scientific™, USA).

2.5 PCR protocol

We tested two different PCR protocols along with two target dilutions. The PCR protocols are given in Figure 6.

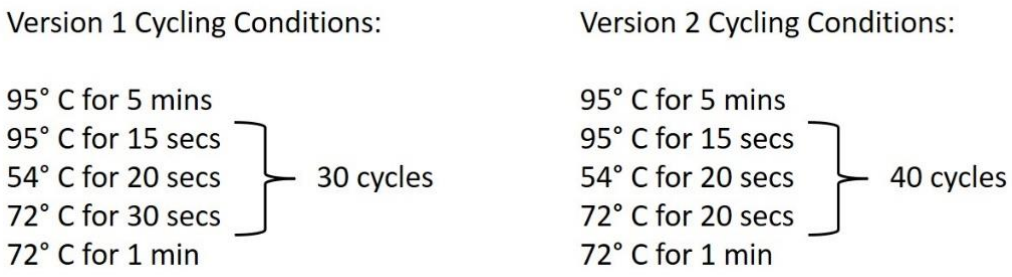

Figure 6 – PCR protocols

For each experiment, six samples were prepared. Three of them were amplified in a conventional PCR machine (T100 Thermal Cycler, Bio-Rad, USA), and others were amplified using our proposed thermocycler. The E-gel results are illustrated in Figure 7 for each test. It should be noted that the lane next to the ladder represents negative control.

The final protocol confirmed for amplification is Version 2 and 100-fold dilution. The bands of this experiment were much brighter than other tests showing the high quality of the PCR reaction. It should be noted that the on-chip system used in these experiments is the final version of the microheater and control system discussed thoroughly in the next chapter (without the micromixer).

The successful amplification performed in all of the on-chip devices proves that no contamination or sample degradation happened inside the reaction well. In addition, compared to

the conventional system, the on-chip system exhibited far brighter signals, which proves the excellent quality of the developed micro thermocycler and control system.

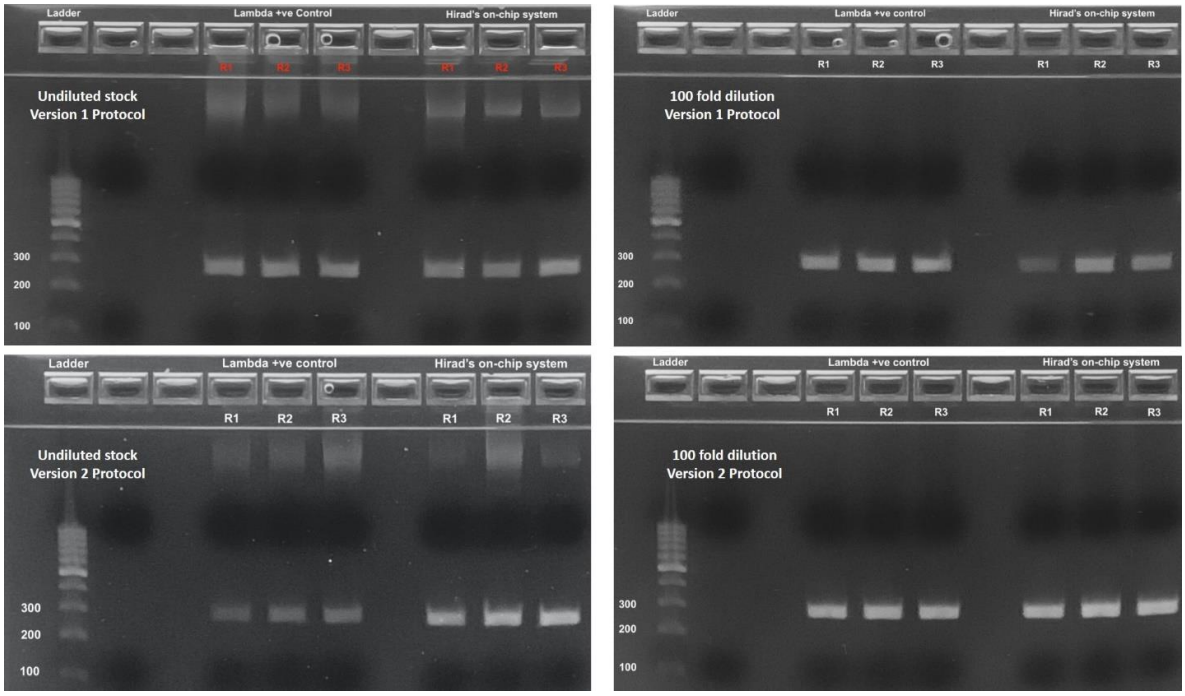

Figure 7 – E-gel results of different protocols and dilutions

Chapter 3: Microheater and control system

3.1 Design considerations

Micro-scaled heaters have been employed in a variety of applications, such as gas sensors [45] and biomedical devices [34]. Thermal uniformity within a region and inside the reaction chamber is crucial for biomedical applications such as PCR. Therefore, the microheater and the temperature sensor must operate efficiently for adequate thermal cycling.

Lab-on-a-chip PCR systems can use external sources to heat the entire structure. These external sources are temperature-controlled blocks [46], Peltier elements [47], infrared lamps [48], infrared laser [49], and other commercial heaters [50] to name a few.

The most significant limitation of using heating blocks is the fact that they have a considerable heat capacity, which slows down the rate at which a sample may be heated or cooled. Block-type heaters have high power consumption and increase the size of the device. In addition, the thermal uniformity provided by block-type microheaters is not satisfactory, particularly towards the edges of the microheaters [51]. Other methods mentioned above need bulky and expensive external components, such as precision optical instrumentation, which are not suitable for developing a low-cost and compact lab-on-a-chip device.

Thermal cyclers for PCR that have a high cooling rate have the potential to drastically cut the overall amount of time needed for the reaction. Therefore, fans or heat sinks are frequently utilized to increase thermal convection or conduction, despite the fact that these components are not absolutely necessary. Because of their huge heat capacity, bulky commercial systems provide a challenge when it comes to the removal of heat. This is often handled by employing a thermoelectric cooler, also known as the Peltier element [52]. For instance, the cooling rate was improved from 1°C/s to 10°C/s when an aluminum heatsink was placed under the PCR chip [53].

Thin film heaters achieve fast heating/cooling rates and effective power consumption because they have low thermal masses and can be fabricated near the reaction chamber. The Joule heating method carries out the thermocycling process in thin film heaters. The temperature gradient is formed inside the PCR reaction chamber as electric current passes through the thin film resistive heater located beneath it.

Platinum [24], [33], [53], [54], gold [41], [55], Aluminum [56], indium tin oxide (ITO) [57], and several thin film heaters have been patterned on microfluidic chips for PCR applications. Thin film Pt has been widely used as a heater due to its high temperature coefficient of resistivity and linear behavior, while the low resistance of gold makes it suitable to be utilized as electrical leads in these devices [58].

In microfluidic chips, it is possible to combine the heater and sensor into a single component. In these chips, sensors are usually narrow and small, with higher resistance compared to the thin film heater to have a fast thermal response [59]. Linear behavior and high sensitivity are desired characteristics in temperature sensors. The significance of fast thermal response intensifies when sensors incorporate into systems with rapid temperature changes, such as in PCR. Platinum's stability and high resistance allows it to be simultaneously used as thin film for heating and temperature sensing in microfluidic devices.

Huang et al. [60] used platinum as a temperature sensor and heating component to perform DNA/RNA amplification. Platinum was fabricated by lift-off on a thin layer of titanium for better attachment to the glass substrate. El-Ali et al. [54] reported heating and cooling rates of up to 50°C/s and 30°C/s, respectively, in their structure which integrated thin film platinum as a heater and sensor. Cui et al. [24] fabricated a separable microfluidic device to amplify DNA. The reusable heater/ sensor section of their design was patterned by magnetron sputtering using Platinum and

Chromium as the adhesive layer. Hsieh et al. [58] proposed an approach to improve the thermal uniformity of microthermal cyclers with array-type heaters. The array-type heater was fabricated using platinum as the heater and sensor, while gold was used as electrical leads. They used a self-compensated function around the edges of the microheater where temperature gradients are noticeable.

Nevertheless, platinum is expensive, and its complicated and dangerous fabrication procedure involving the lift-off process [61] and wet etching in toxic aqua regia [62] complicates its incorporation in microfluidic PCR devices. The properties of gold and its compatibility with glass made it an ideal choice for a microheater in our device. Patterning a platinum sensor alongside a gold heater is complicated, and given its high cost, it is impractical for our device. In addition, although other metals may also behave linearly, their low resistance reduces the sensing accuracy [61].

In this chapter, we will first introduce the designs for microheater electrodes, followed by their fabrication. The temperature control system is elaborated on next. The performance of the microheater and control system are discussed using several parameters.

3.2 Design

Temperature cycling is performed by heating and cooling the PCR mixture using a specific protocol. Joule heating method carries out the thermocycling process in the microfluidic device proposed in this study. Achieving uniform temperature distribution over a designated area is the prime concern in developing microheaters. The pattern design of the electrode plays a crucial role in addressing this concern, and studies have been made to find an efficient heater layout.

Geometries with meandering narrow line electrodes are generally incorporated into microfluidic devices since they reduce power consumption [55], [63]. The edges of these designs

usually experience lower temperatures leading to nonuniform temperature distribution in meandering structures. As a result, the heater should cover a region larger than the reaction chamber to compensate for this non-uniformity. In order to improve the uniform heating of meandering patterns, narrow electrodes in spiral shape are suggested [55], [63]. The preliminary designs for the microheater are shown in Figure 8.

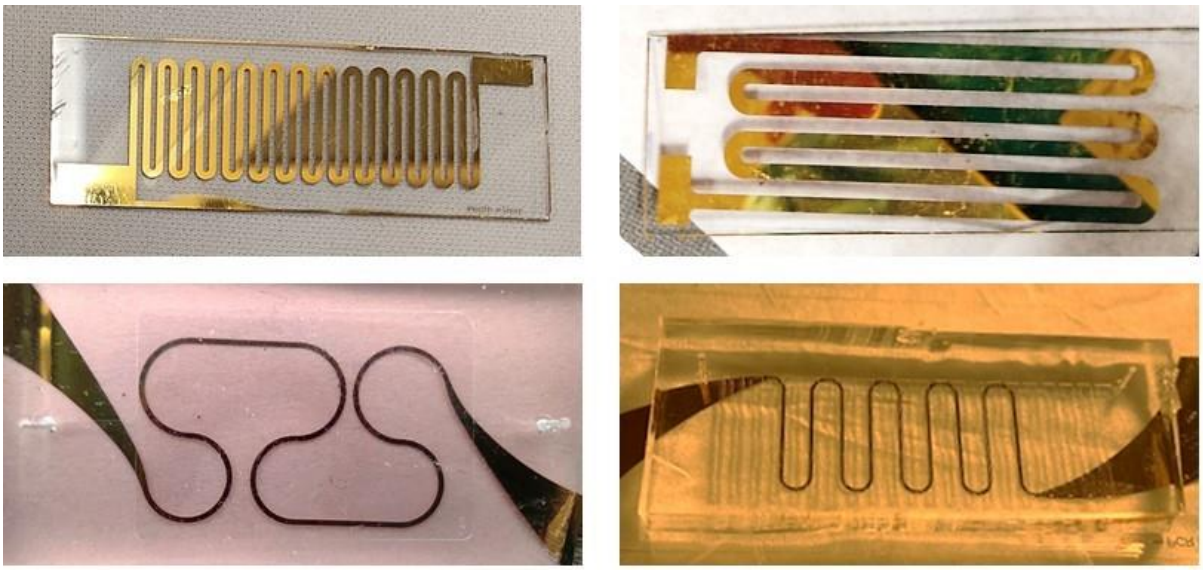

Figure 8 – Preliminary microheater designs for simple and serpentine PCR chamber

The microheaters were created via photolithography by patterning gold on glass which will be thoroughly explained later. These patterns were proposed to be used in preliminary PCR reaction chambers. The pictures on the down left and down right demonstrate these designs bonded to a simple rectangular reaction chamber and a serpentine reaction chamber, respectively. After deciding to choose PCR reaction well over PCR chambers, heater designs were also profoundly modified.

The modified designs were aimed to provide temperature uniformity with ±1 °C precision across a circular area that houses the PCR well. The design also focused on providing fast thermal

response times while lowering the power required to heat the electrodes. In order to accomplish these goals, the size of the electrodes and the distance between them were gradually optimized by conducting several experiments until satisfactory results were achieved.

Figure 9 shows the patterns designed for heating PCR reaction well. The edges of thin-film heaters always show lower temperatures compared to the middle region because of low ambient temperature. One approach that has been implemented to address this issue is to increase the resistance in the corners of the heater [58]. However, this idea complicates the design of the pattern and its fabrication as well. A more straightforward solution to this problem is to have the heater cover a larger area than the target region. In all proposed designs, the heating region can be fitted into a square with a side length of 1 cm.

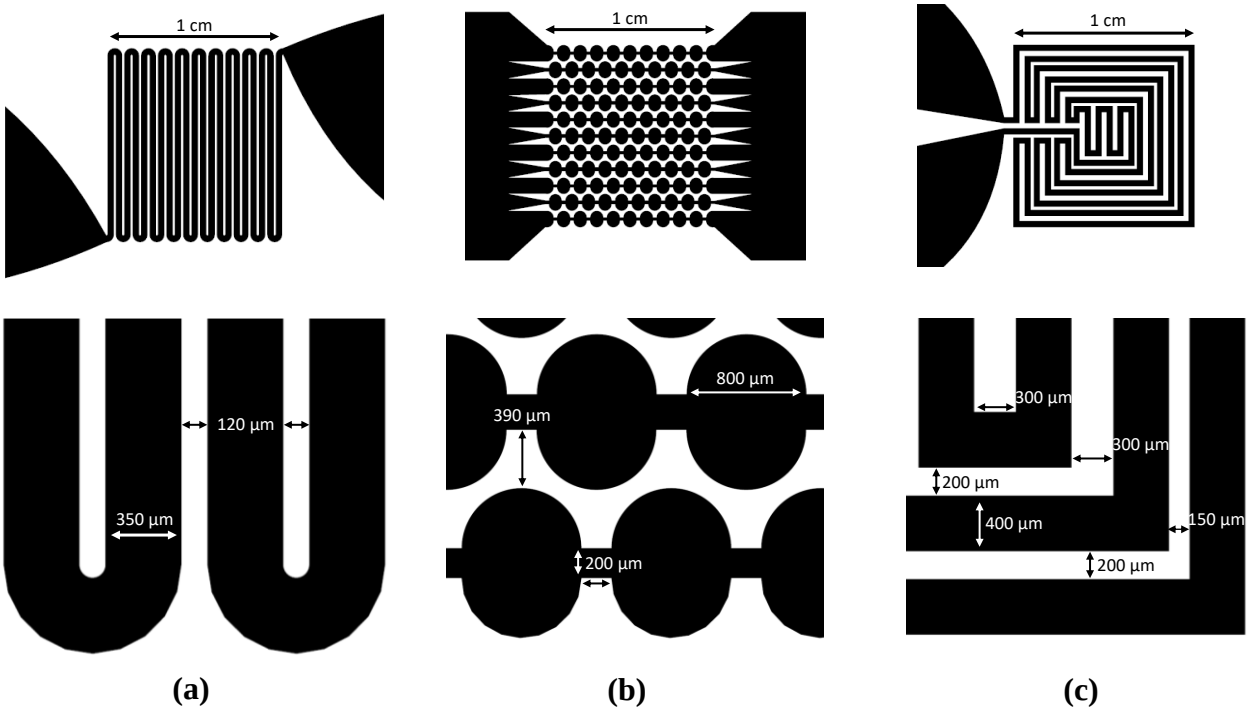

Figure 9 – Heater patterns designed for microheater and detailed dimensions. (a) Design 1, (b) Design 2, and (c) Design 3

The electrodes' width, total length, and electrode spacings are factors involved in power consumption and heating uniformity. For instance, by reducing the spacings between heaters, the heated region is better covered by the electrodes. Designing wider electrodes would decrease their resistance and make them appropriate for fast heating, although the effect of electrode's length should also be considered. Designs in Figure 9 were also investigated with other electrode dimensions as well to find a sufficient compensation between power consumption and temperature uniformity. An infrared imager was used to investigate temperature uniformity.

3.3 Fabrication

Figure 10 demonstrates few steps of microheater fabrication. The pictures were taken inside class 100 clean room facility (Applied Micro & Nanosystems Facility, University of British Columbia, Okanagan Campus).

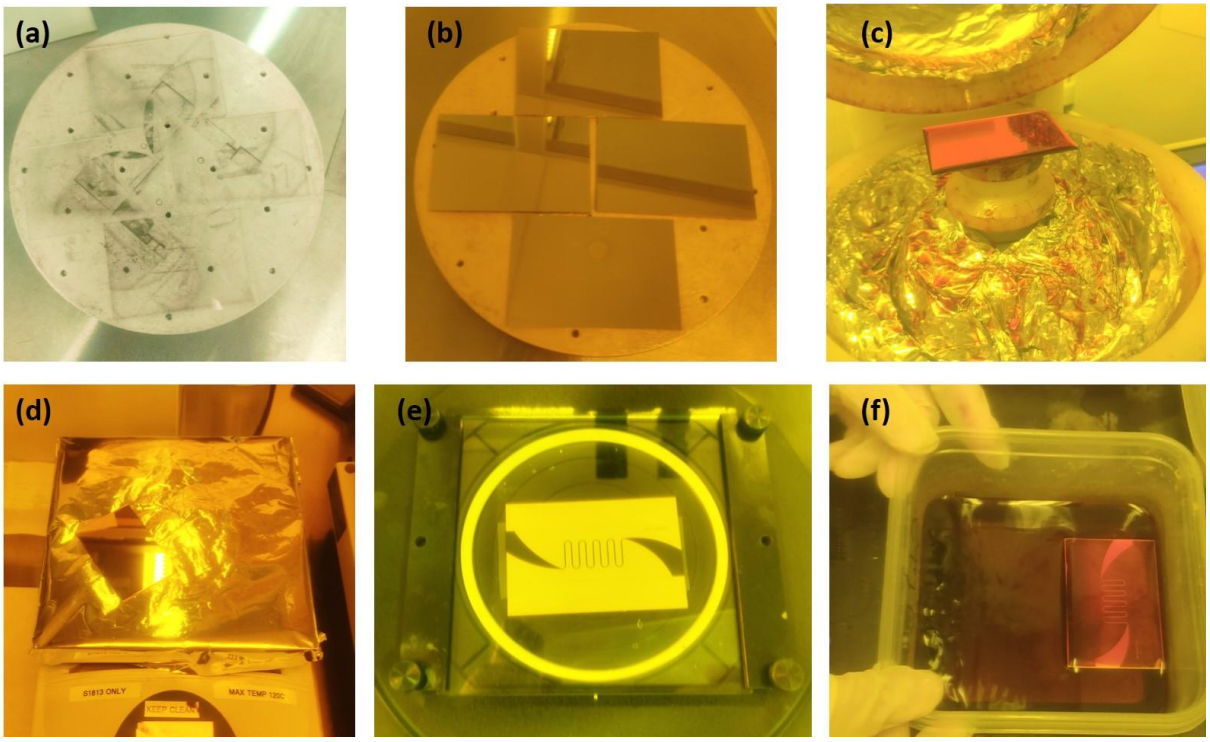

Figure 10 – Several fabrication steps of microheater. (a) Glass slides on sputtering machine tray. (b) glass slides after gold deposition. (c) S1813™ photoresist poured on gold deposited glass slide inside spin coater. (d) Soft bake process. (e) Mask aligner, and (f) UV exposed glass slide inside gold etchant

Glass slides were first deposited with gold in the sputtering machine. The thickness of gold is 1000 Å, and 100 Å chrome acts as the adhesion layer. Positive photoresist (MICROPOSIT™ S1813™ G2) was spin-coated on the slide at a spin speed of 500rpm for 10s and a spread speed of 3000 rpm for 20s. The glass slide was then soft-baked at 115°C for 2 min. For transferring the heater pattern, the mask layout was designed using a CAD program, and UV exposure was carried out for 8s under a wavelength of 365 nm and 20 mW/cm^2 (Model 204IR, OAI). Then, the photoresist was developed for 45s in developer (MICROPOSIT® MF®-319). To perform the wet etching process, the glass slide with patterned photoresist was immersed for 30s into a gold etchant (TFA gold etchant, Transene). To remove the unwanted chrome layer, the glass was immersed in chrome etchant (TFE chromium etchant, Transene) for 10s. The residual photoresist was then stripped by MICROPOSIT™ REMOVER 1165. At the final stage, the glass was rinsed with water and isopropanol (IPA) and dried with nitrogen gas. Figure 11 presents the fabricated heaters.

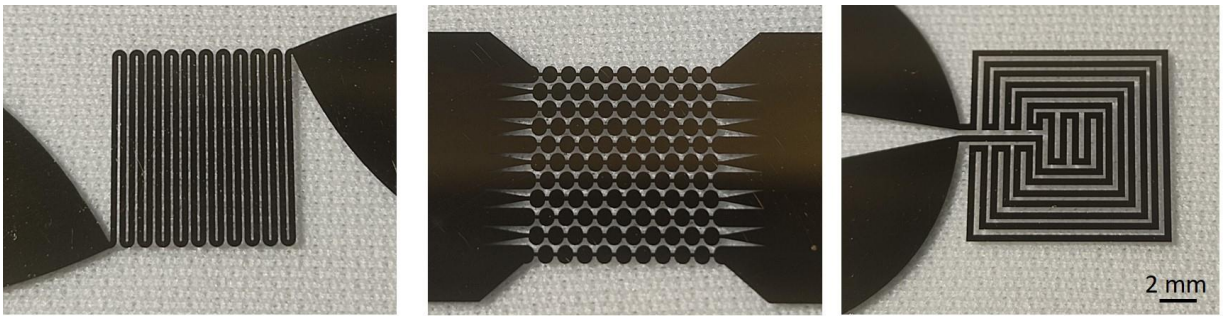

Figure 11 – Fabricated microheaters. (a) design 1, (b) design 2, and (c) design 3

3.4 Temperature control system

The cycling protocol in PCR reaction includes three stages: maintaining a steady temperature, cooling, and heating. These steps are automatically mediated with the help of a microcontroller. The microheater is connected to the power supply using crocodile connections

(B&K Precision Corporation, Model 1672) through the microcontroller. The power supply operates on constant voltage mode while the controller monitors the time of thermocycling stages and temperature inside the reaction well. The programmable controller provides tuned voltage to the heater based on the feedback from the sensor as the temperature set points are altered according to the algorithm. Figure 12 illustrates the schematic of the temperature control unit.

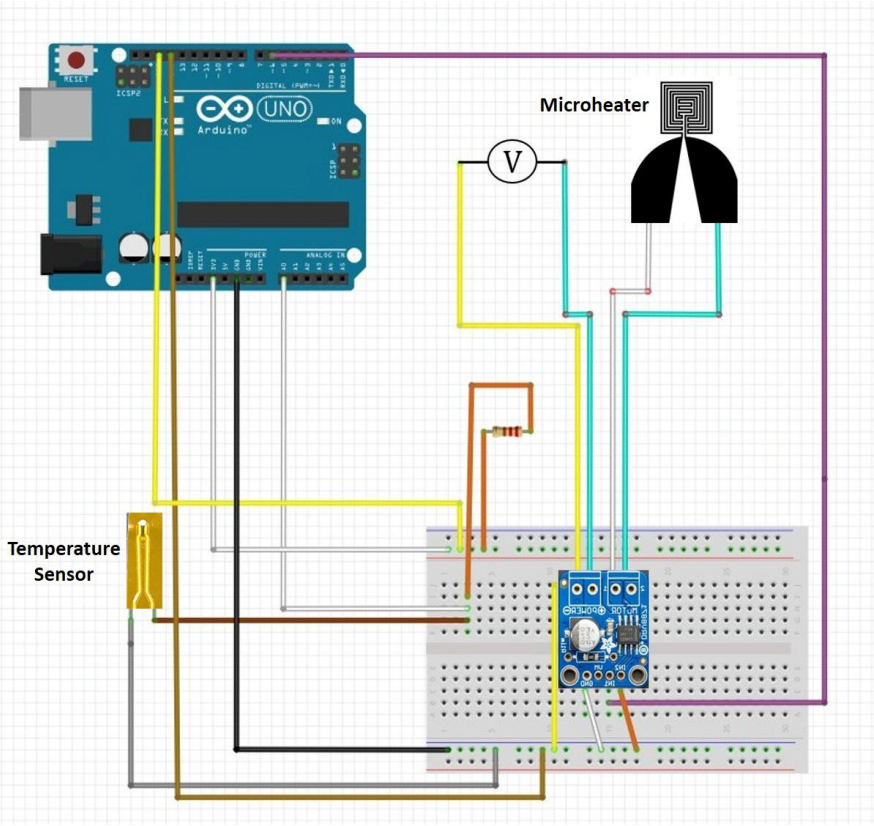

Figure 12 – Schematic of the temperature control system

It is crucial to verify that the measured temperature correlates with the actual temperature distribution of the PCR mixture in order to ensure an accurate and repeatable amplification. Nonetheless, it is not a good idea to monitor the temperature inside the reaction well during PCR amplification by embedding a sensor inside it. PCR reagents are highly sensitive to contamination,

and the presence of a non-biocompatible object can affect the result of amplification leading to loss of target DNA and reagent waste. In addition, the load effect of the external sensor makes temperature measurement inaccurate [64]. Non-contact measurements are also inappropriate since the top of the PCR mixture is covered with mineral oil.

As discussed before, integrated thin film sensors were not an appropriate option for our device. Surface thermocouples are costly as well. However, thermistors were a suitable option due to their cost, precision, stability, size, and compatibility with microcontrollers. A 10KΩ thermistor (B3950 NTC) with a negative temperature coefficient was purchased from Adafruit. Non-linear resistors, known as NTC thermistors, have resistance characteristics that change in response to changes in temperature. In other words, the thermistor's resistance will drop as the temperature rises. With the help of a thermal conductive tape, the sensor is attached to the backside of the glass slide patterned with heater electrodes.

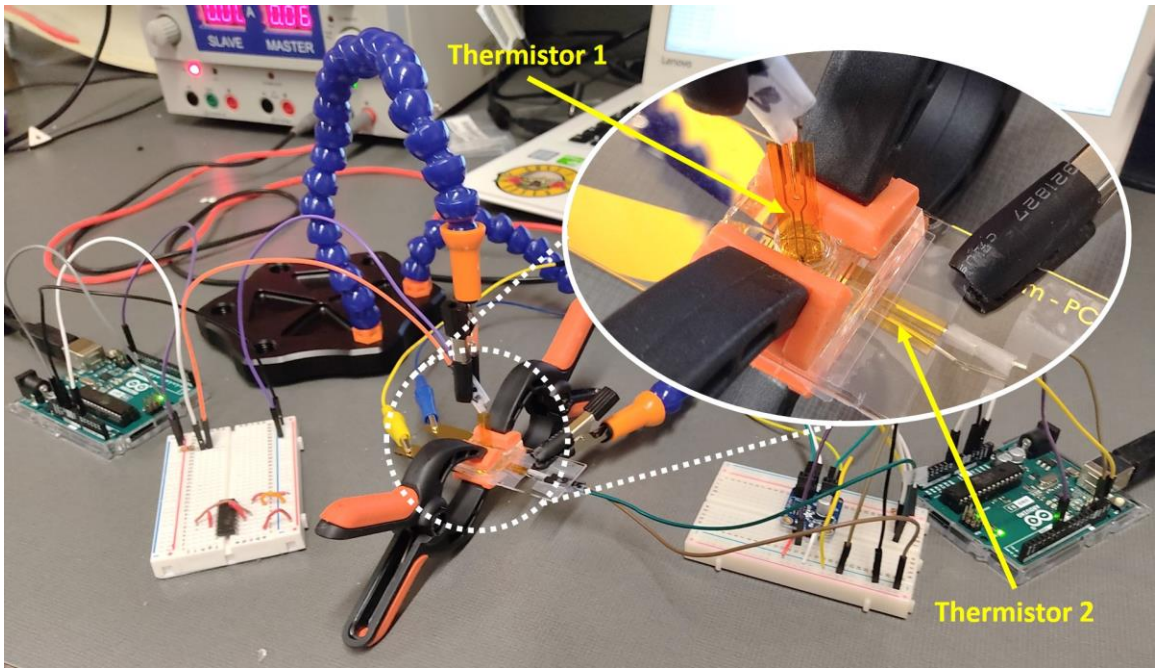

Figure 13 – Calibration of temperature sensor

This temperature sensor was thermally calibrated to report the temperature inside the well. Although small thermal mass of the chip allows rapid heat transfer, precise measurements can improve the quality of amplification. For calibration, first, a small bath of DI water was prepared. The temperature was measured by a thermistor (thermistor 1) and a calibrated thermocouple inserted inside the bath for temperature set points from 40°C to 98°C.

Then the calibrated thermistor (thermistor 1) was inserted into the reaction well as shown in Figure 13. The thermistor to be used in final device (thermistor 2) is then attached to the back of the glass. It was calibrated to show the temperature inside the reaction well using the embedded temperature sensor (thermistor 1). Sufficient time was provided to the DI water inside the well to reach and stabilize temperature at set points from 40°C to 98°C to increase accuracy. The size of the reaction well used here is the same as the one used for the ultimate integrated device. The thermocouple probe was too large to be utilized directly for calibration.

3.5 Results and discussion

This section provides the results for thermal performance and control system of the device. The temperature uniformity of the proposed heater patterns is analyzed first. Then, in accordance with the suitable design, the diameter of the reaction well is decided. To analyze the control system, the performance of the device in maintaining temperature and thermal ramping/ cooling responses is studied.

3.5.1 Temperature uniformity

The heaters are designed to create uniform heating and fast thermal response with low power consumption. Temperature uniformity in an area can be defined as where the temperature difference between set point temperatures is less than 1 and/ or 2°C [65]. The spatial thermal

uniformity of the proposed designs was verified by an infrared imaging system, and their performance was compared over circular areas.

Surface emissivity and its distance from the camera are critical parameters in IR measurement accuracy. However, despite the exact value of surface emissivity being unknown, this method is effective for showing temperature fluctuations with high resolution [56]. As gold directly reflects infrared light from its surroundings, an image taken with the resistor facing the IR camera would show a heat map of the surroundings rather than the actual temperature of the electrodes [55]. Therefore, images were taken from the backside of the glass patterned with heater electrodes. Figure 14 illustrates the images taken by IR camera (FLIR Flip 4) from three different heater designs at the temperature of 95°C (denaturing temperature).

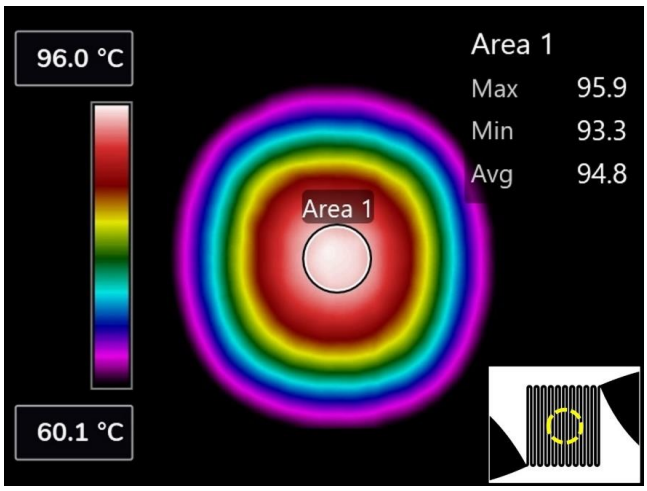

(a)

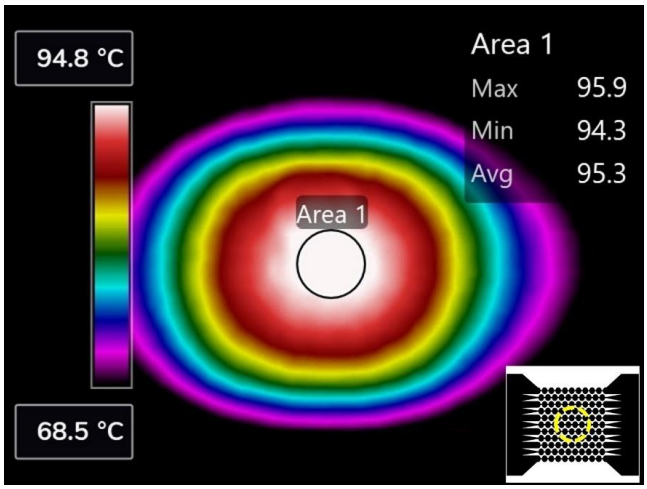

(b)

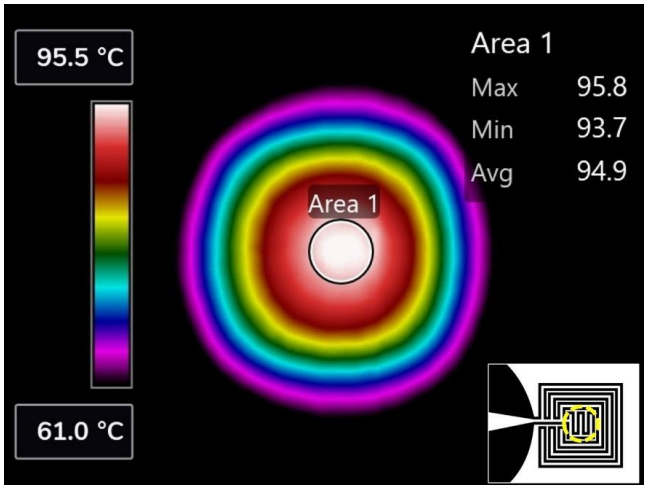

(c)

Figure 14 - IR images of heater designs at 95°C. (a) design 1, (b) design 2, and (c) design 3

IR images shown above are processed by FLIR postprocessing freeware. The performance of heaters was compared using the freeware over circular regions. Area1 demonstrated in IR images of Figure 14, is a circle of 4 mm in diameter.

It can be observed that the overall shape of heating maps in designs 1 and 3 are pretty similar. Their heating maps are almost fully symmetric, while the heating map in design 2 is

somehow stretched. Design 2 maintains higher average temperature distribution outside the main heating region, probably because of the narrow electrodes on two sides of this region.

Design 2 suggests the lowest temperature deviation in Area 1. Numerous small nodes with small distances from each other could be the reason for not allowing large heat dissipations from edges and the temperature to drop below 94.3°C, while other designs showed minimum temperatures below 94°C in Area1. Design 1 reported the most deviation due to the high thermal dissipation from its edges, whereas in design 3 the center of the heater is surrounded by electrodes to avoid heat dissipation. With the help of these electrodes, design 3 showed the best performance on average temperature. Evidently, as the area gets bigger, this average value and minimum value drop.

The width of electrodes in design 1 is 0.35 mm which are located 0.12 mm from each other. In design 3, the electrode width is 0.4 mm. The resistivity of designs 1, 2, and 3 were 260 Ω, 10 Ω, and 90 Ω, respectively, at room temperature. Although design 1 shows good thermal uniformity with an average of 94.8°C, it required around 14 V to reach 95°C. On the other hand, design 3 needed around 8.1 V. This voltage difference increases power consumption and makes integration of design 1 into a portable lab-on-a-chip device much more complex. These two designs were tested with other dimensions as well. Usually, increasing the width reduced temperature uniformity, and decreasing it increased power consumption rapidly while not improving temperature uniformity significantly. For example, design 3 with 0.2 mm electrodes needed around 20 V to reach 95°C because of its pretty high electric resistance.

Design 2 had the lowest power consumption. It needed only 1 V to reach 54°C and 1.8 V to reach 95°C. Although this might sound pretty satisfying for a heater, it might not work well for a thermocycler. A small alteration in voltage drastically changes the spatial temperature, making

temperature control challenging. Moreover, fast heating ramps do not allow sufficient thermal distribution inside PCR mixture, impacting the quality of amplification. Same performance analysis on circular regions with different diameters almost presented the same results. Considering these explanations, design 3 appeared to be the best fit for the heater pattern.

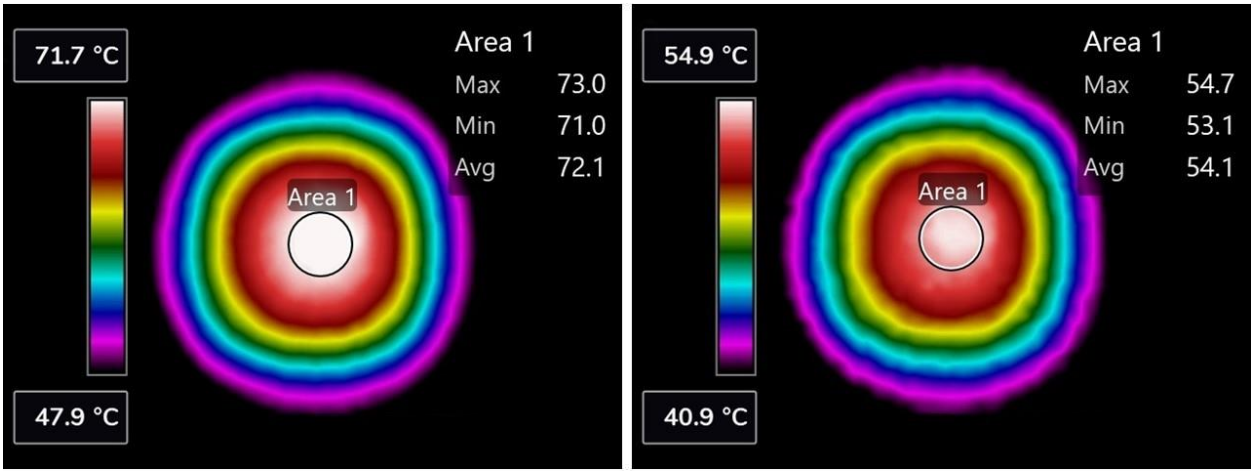

(a) **(b)**

Figure 15 – IR images of design 3 at (a) 72°C and (b) 54°C

Figure 15 displays the spatial thermal uniformity of design 3 at 72°C and 54°C, which are extending and annealing temperatures, respectively. It can be seen that as the temperature rises the deviation of maximum and minimum temperatures from the desired set point intensifies. This happens due to the fact that heat dissipation to the surroundings becomes easier and larger as the temperature difference with the ambient increases. However, the average temperature is highly satisfying and design 3 demonstrated similar heating map patterns over the designated temperatures proving temperature uniformity over the desired area.

3.5.2 Well diameter

After choosing the suitable pattern for the electrodes of the heater, the appropriate diameter of the reaction well must be found. The reaction well is located above the microheater, and heat transfers to the well by Joule heating as illustrated in Figure **16**.

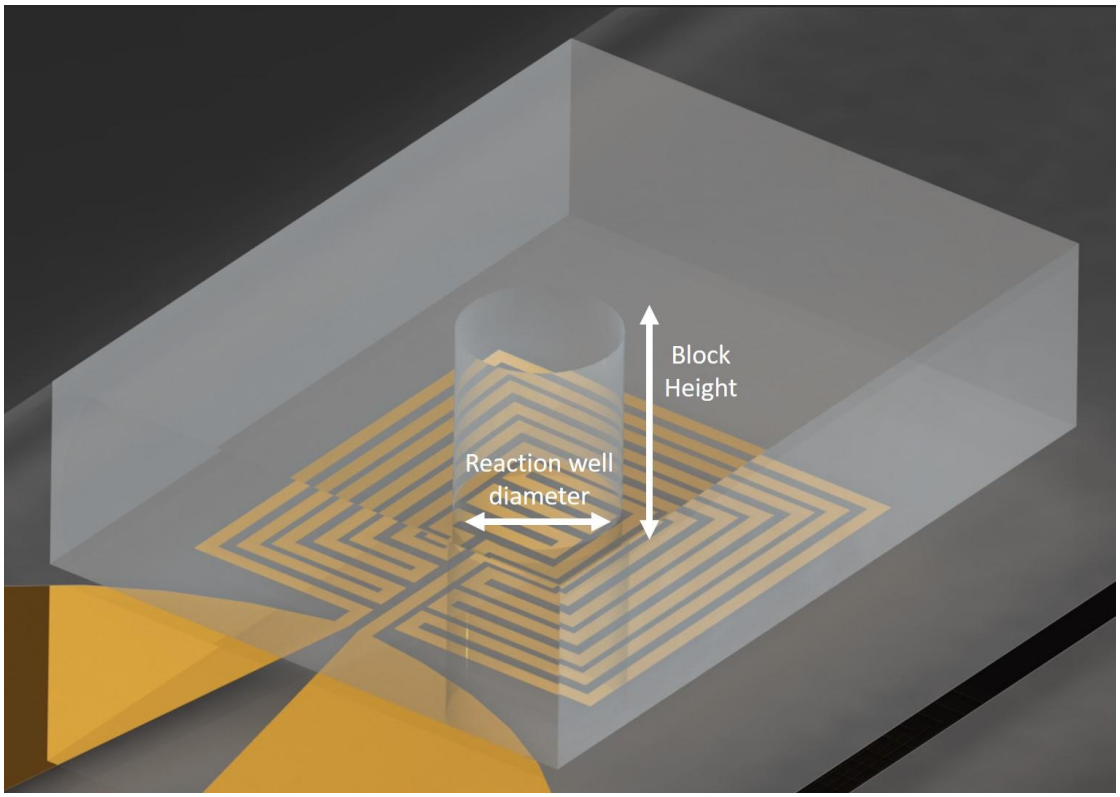

Figure 16 – Reaction chamber well block located on top of microheater

Fast thermal distribution and uniform temperature are key parameters in successful PCR process. Therefore, two main points must be considered when choosing the well diameter. First, the heater cannot provide uniform heating over a vast area. And second, attaining homogeneous temperature distribution requires more time as height increases. In other words, as the diameter gets smaller, temperature uniformity increases across the diameter, but uniform thermal distribution along the well's height might not occur. Table 1 provides details on well diameters and

corresponding mixture heights. The total height column represents the height of the PCR mixture covered with mineral oil to avoid evaporation. In other words, it represents the minimum block height required.

Table 1 – well diameters and corresponding mixture heights inside the reaction well

Sample volume (µL)	Well diameter (mm)	PCR mixture height (mm)	Total height (mm)
20	3	2.83	4.24
20	3.5	2.08	3.11
20	4	1.59	2.38
20	4.5	1.25	1.88
20	5	1.02	1.52
20	5.5	0.84	1.26

As discussed before, measuring temperature inside the reaction well at different heights would be inaccurate due to the load effect of the external thermometer. Also, thermometers or thermocouples with this precision are expensive. Therefore, it is tried to find a satisfactory compromise between height and temperature uniformity across the circular area of the corresponding diameter.

To achieve this, IR images were analyzed using FLIR freeware. Images were captured at 95°C since highest deviation from desired setpoint happened at this temperature. The temperature uniformity was analyzed inside three circular areas with diameters of 3.5, 4.5, and 5.5 mm. These diameters are illustrated in Figure 17 with D1, D2, and D3 annotations, respectively.

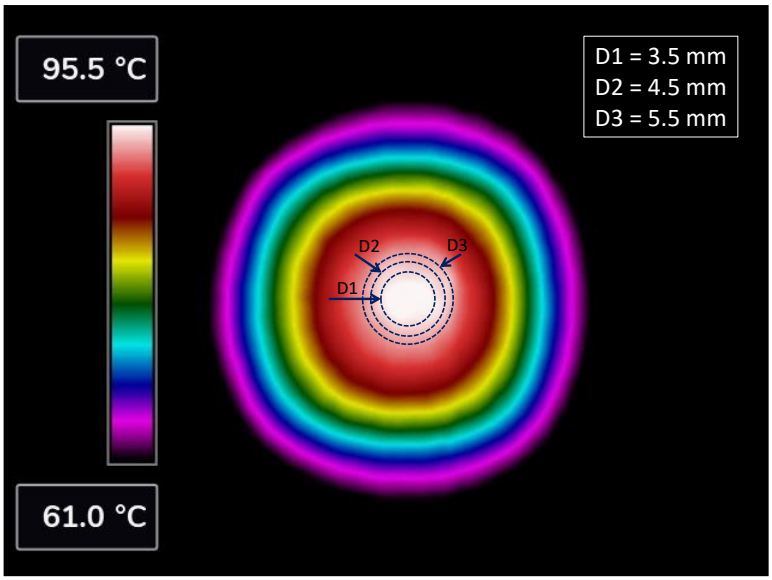

Figure 17 – Different well diameters inside the selected microheater (design 3) at 95°C

We considered the span of ±1°C temperature difference as uniform. The uniformity is then reported as the percentage of points inside this temperature span. For instance, at 95°C, the uniformity of D3 would be the percentage of areas with temperatures between 94°C and 96°C.

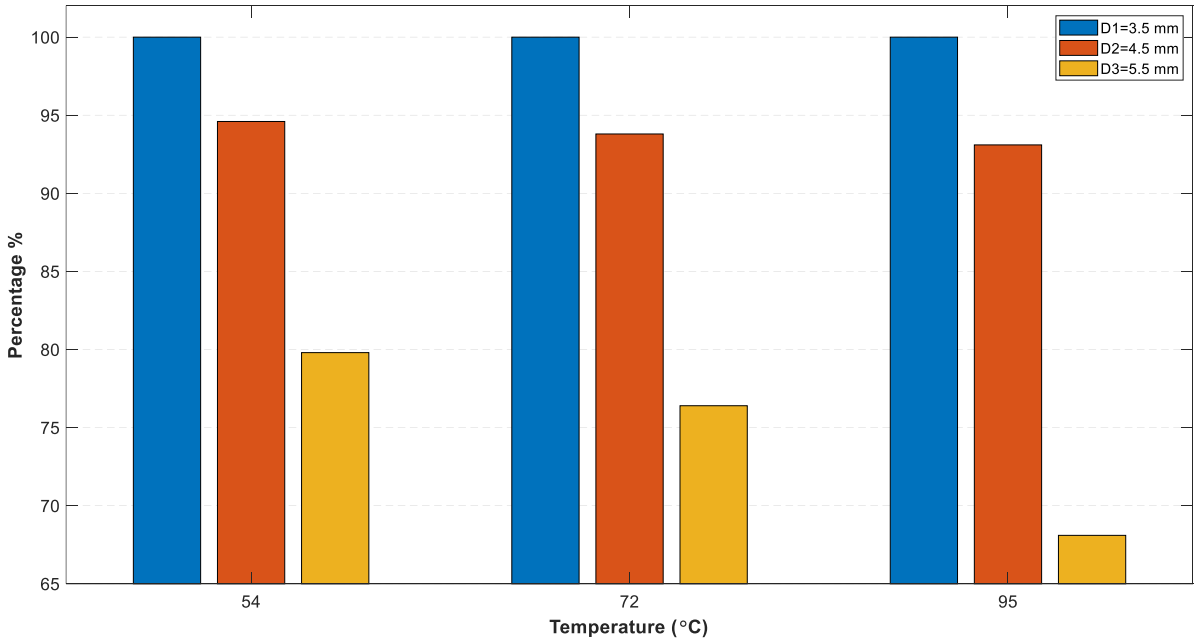

Figure 18 – Uniform area percentage inside different well diameters with ±1°C accuracy

The bar charts in Figure 18 show the percentage of temperature uniformity as defined for different diameters at PCR protocol temperatures. D3 shows unfavorable results with temperature uniformity of 68 % at 95°C. D1, on the other hand, suggests superior performance by 100% uniformity at all temperatures. However, the PCR mixture would have a height of 2.08 mm at this diameter which is 66 % higher than the height for D2.

Furthermore, the total height of the reaction well block will be affected as well. Our device is aimed to be low-cost and disposable, where fabricating blocks with large heights would increase the cost of material (PDMS) used. D2 suggests satisfactory uniformity, which is not affected by temperature alterations. Temperature uniformity at 95°C is equal to 93.1%, which is pretty high. However, we decided to choose the final well diameter of 4 mm to be safe with temperature uniformity. Also, the height difference between D2 and a diameter of 4 mm is not that significant compared to D1.

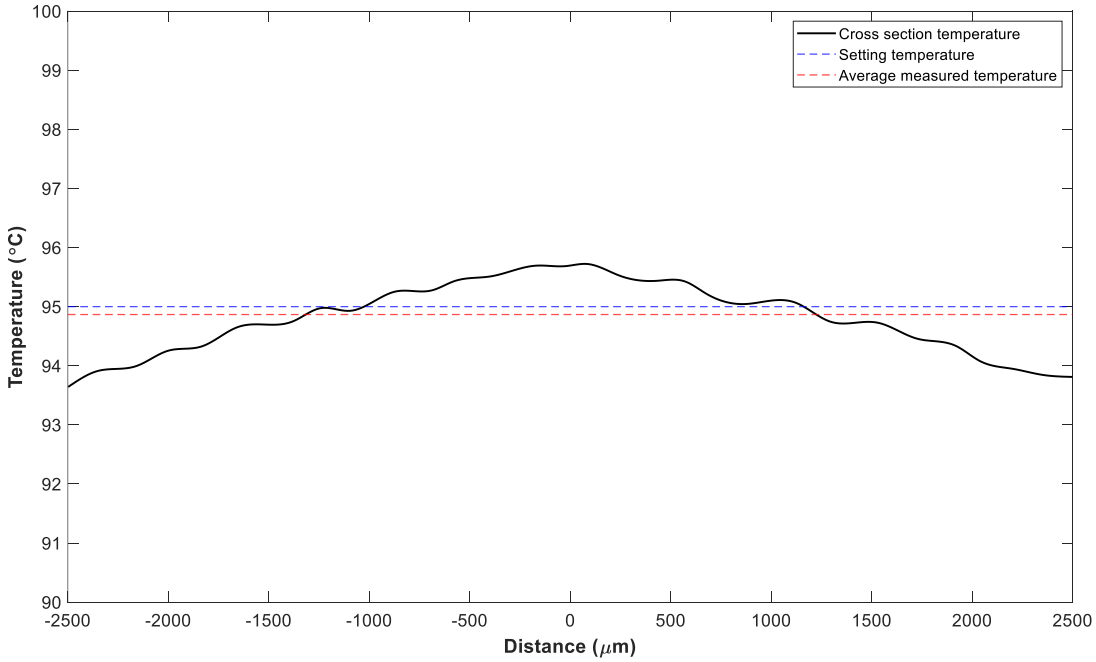

Figure 19 – Cross-section temperature distribution of selected heater at 95°C

Figure 19 is presented to better understand temperature fluctuations inside the circle of D2 at a temperature of 95°C. The plot shows the temperature along a horizontal line crossing through the heated region. The maximum temperature is 95.8°C, as illustrated before in Figure 14c. Large drops in the plot are probably due to the regions which are not covered by the heater electrodes. The temperature decreases by moving from the center of the heater toward the edges. The rate of drop in temperature increases as we get closer to the edges of the heater. Next section will investigate the performance of the temperature control system.

3.5.3 Heating/cooling performance

In previous sections, the performance of the heater was studied. For successful PCR amplification, the temperature of the PCR mixture must be carefully controlled and regulated. Therefore, this section provides the performance of the control system on monitoring the temperature inside the reaction well. PCR protocol consists of repeated increases and decreases in temperature while the control unit must be able to maintain the temperature at specific temperatures with the lowest possible fluctuations. PCR reagents are highly sensitive to temperature and the quality of amplification will be reflected if the protocol is not followed properly.

Our control system is designed to work at any temperature inside the ordinary working range of PCR protocols. To achieve this, sufficient number of tests were conducted. In each test, two arbitrary set points were designated. The performance of the control system was investigated for both heating and cooling between these set points followed by maintaining the temperature for around 15 seconds.

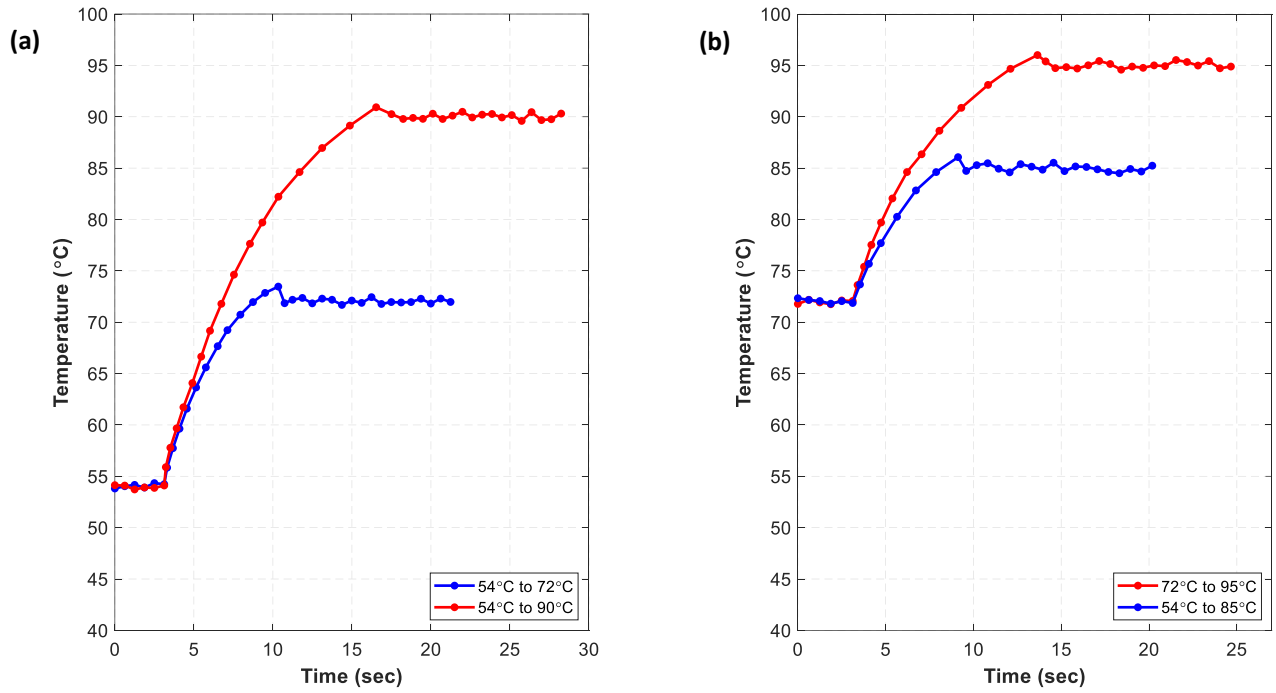

Figure 20 – Heating and temperature maintaining performance of the microheater. (a) Heating from 54°C to 72°C and 90°C, (b) Heating from 72°C to 85°C and 95°C

The results for heating performance are reported first. As an example shown in plots of Figure 20, 54°C and 72°C which are common PCR temperatures for annealing and extending are designated as start set points. Two arbitrary setpoints were chosen for each of these temperatures to analyze heating performance.

The evaluated heating rates were usually between 2 and 2.6 °C/s depending on two main factors. First, higher heating rates are observed in lower temperatures because uniform temperature distribution inside the well occurs more quickly. Second, the heating rate decreases as the difference between the two set points narrows.

Although in previous sections, heater design and well diameter were selected in a way to facilitate thermal uniformity inside the well, the control system must also allow sufficient time for the reaction well to reach uniform thermal distribution. This is a crucial concern since each PCR

step requires a specific dwell time. The control system of the proposed device prevents the heater from rapid ramp rates to address this concern. In this regard, overshoot and undershoot in heating and cooling are among the other most common solutions proposed for thermocyclers.

According to the plots, the temperature difference after reaching the desired set point is lower than 1°C, which can be regarded as uniform. The microcontroller is programmed to act super cautiously around the temperature of 95°C since large deviation from this temperature may result in boiling the mixture due to its high aspect ratio and low volume.

Figure 21 displays the cooling performance of the device in two separate plots. The set points for each plot are different.

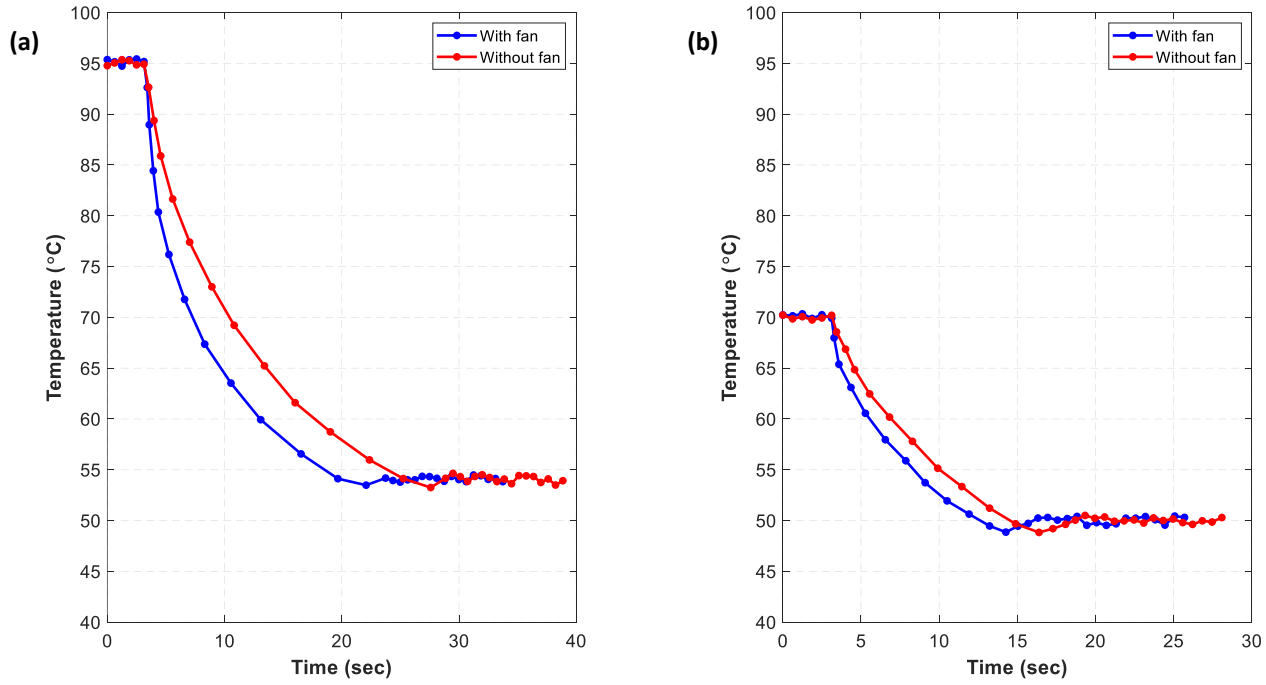

Figure 21 – Comparison of cooling and temperature maintaining performance of the microheater by utilizing fans (a) Cooling from 95°C to 54°C, and (b) Cooling from 70°C to 50°C

Here, the performance of the device is compared to when fans are employed as well. Two fans (Delta Electronics, AUC0512, 20.2 CFM) were placed at the bottom of the microheater to

facilitate cooling. The average cooling rates are smaller than the heating rates. Evidently, utilizing fans would increase the cooling rate. The highest cooling rates recorded were 2.1°C and 1.7°C for the device with fans and without fans, respectively. These rates were recorded between the denaturation and annealing steps of the protocol chosen for our application.

Considering the cooling rate difference between using and not using fans we decided against including it in our device. Utilizing fans decreases cycle time by around 5 seconds which is not that significant. However, it would be an extra component that not only increases the size of the whole microfluidic device but also increases its power consumption.

Overall, it can be said that the control unit works adequately to maintain the temperature at desired set points with low deviation. Also, the heating and cooling rates are acceptable and ensure uniform thermal distribution inside the reaction well.

Chapter 4: Micromixer

4.1 Design considerations

Quick and efficient reagent mixing is essential before conducting bioengineering and biochemical systems tests such as drug administration [66]. In general, mixing in the macroscopic domain is turbulence. However, mixing in the microscale often occurs as a result of molecular diffusion processes. The low molecule diffusivities would make fluid mixing extremely challenging [67]. For example, consider a microchannel with a width of 100 μm. The Reynolds number would be equal to 0.1 when water (viscosity of 0.001 $N \cdot s/m^2$ and fluid density of 1 kg/m^3) flows through the channel at a rate of 1 μL/s. It would take the fluid one thousand seconds to diffuse one millimeter. Therefore, to increase the mixing rate, it is necessary to use special devices: micromixers.

A micromixer is a device for mixing micro- and nano-liter volumes of fluids in a microscale channel. Micromixers are essential components of lab-on-a-chip devices because high-throughput and advanced systems demand effective mixing strategies. The mixing power of micromixers can impact how well a system works as a whole in a variety of microfluidic applications. Micromixers have the ability to generally incorporate mixing, detection, and separation onto a chip that is centimeter-level or smaller. Chemical reaction, polymerization, and biological analysis are just a few common applications of micromixers in biomedical systems [19], [68], [69].

Micromixers, as one of the essential components in microfluidic devices, significantly influence the effectiveness and sensitivity of biomedical microsystems, and PCR amplification is no exception. Mixing is often carried out by pipetting, a tedious and time-consuming process that is highly dependent on the technicians' working skills. It is prone to contamination, and human error in reagent handling interferes with amplification quality [70]–[72]. Here, we tried eliminating

these unfavorable issues by mixing the target with the reagents inside a disposable and autonomous micromixer.

Micromixers may reach high mixing efficiency at any Reynolds number depending on their geometries, mechanism, and external actuators. Micromixers are classified into two types based on their mixing mechanism: passive and active devices. In contrast to active microfluidic devices, which rely on external energy sources for mixing, separation, etc., passive microfluidic devices do not require any external actuator to drive the fluids. Regarding efficiency and mixing time, each group has its own set of benefits and drawbacks [73], [74].

4.1.1 Active micromixers

Active methods rely on the employment of various external fields and the change in the fluid flow rate. By expanding the contact area between the fluids or causing chaotic advection, external energy sources are utilized to improve the mixing quality. In literature, external energy sources are divided into these main categories: Pressure field, sound field, magnetic field, and electrical field [75], [76].

Micromixers that are driven by a pressure field often have simple designs, with just two cross channels or a main channel and one or more side channels. By utilizing fluid stretching and folding, Niu and Lee [77] created a pressure-driven micromixer that created chaotic mixing, and they optimized their design with the help of the Lyapunov exponent.

Acoustically induced disruption in micro streams is the basis for sound field-driven micromixers. Ultrasonic transducers, thin-film piezoelectric devices, and surface acoustic waves (acoustic waves that pass along the surface of a solid) are only some of the technologies that have been used to implement acoustic resonant disturbance. Luong et al. [78] deposited focused interdigitated electrodes on a piezoelectric substrate to generate surface acoustic waves, resulting

in acoustic energy concentration. It has been found that focusing electrodes have a higher mixing index than standard parallel electrodes.

Micromixers that are powered by a magnetic field rely on magneto-hydrodynamics but can also be activated by a permanent magnet, electromagnet, magnetic stirring, or integrated electrodes. Ferrofluids are extensively employed for studies on magnetic micromixers. A ferrofluid-based magnetic mixer was created by Nouri et al. [79] to study the mixing of deionized water and Fe_3O_4 ferrofluid in a rectangular cross-sectional Y-mixer channel with a permanent magnet. Under the magnetic field created by the permanent magnet, the ferrofluid traveled from the bottom of the channel to the top, causing a mixing of the two fluids.

In order to create an electrical field-driven micromixer, electrohydrodynamic disturbance and electrokinetic instability are used. Electrically charged fluids moving in an alternating or direct current (AC or DC) electric field disrupts the interface, resulting in improved mixing performance in micromixers. A Y-mixer reported by Huang et al. [80] featured an array of inclined electrodes on the bottom of the main channel. In order to improve mixing, they used AC signals to create electro-thermally induced vortices in the electrolyte above the corners of the electrodes. The authors discovered four vortices form above each electrode pair, with two strong vortices remaining for a long time and two weak vortices canceling out.

4.1.2 Passive micromixers

Passive micromixers use intricate channel geometry but do not require an external energy source like their active counterparts. Mass transport in passive micromixers occurs through molecular diffusion and chaotic advection, both of which can be amplified by increasing the contact area between the fluids. In order to minimize the diffusion length and increase the

interfacial area between the fluids, chaotic advection is typically produced by altering the microchannel's structure [81], [82].

The structural dimensions of passive micromixers divide them into two distinct categories: three-dimensional (3D) and two-dimensional (2D) designs. In order to improve mixing, 3D passive micromixers frequently rely on complicated spatial structures that are difficult to fabricate and capable of generating a wide range of vortices (including second flow vortices, Dean vortices, chaotic advection, etc.). In literature, each of these subgroups was also categorized into different types. Here a few examples of each type will be explored.

For instance, to boost the mixing efficiency of chamber-based 3D passive micromixers, chambers with specific structures, including convergence-divergence structures, recirculation structures, and counterflow structures, are frequently utilized. These multi-lamination patterns include multilayer structures in which fluids enter the mixer in a variety of arrangements, including diverse forms such as L-shape[83], C-shape[84], H-C-shape[85], and H-shape[86] respectively. By splitting and then recombining the two fluids to be mixed, Nimafar et al. [86] were able to design an H-shaped micromixer that maximizes diffusion. At Re=0.083, the fluid in the channel folded, rotated, and expanded, resulting in a mixing efficiency of 0.98. This was made possible by the splitting-recombination process.

3D Spiral Based Micromixers are another well-known subgroup of 3D micromixers. The design reported by Rafeie et al. [87] features 3D spiral and fine-threaded microchannels. Both chaotic advection (caused by the presence of Dean flow) and diffusive mixing (facilitated by the thread-like grooves encircling the curved body of the mixers) played a role in the development of the design. The Dean number is a dimensionless parameter that describes the fluid flow in curved-

based micromixers [74]. They showed a micromixer that was effective across a broad range of Reynold numbers (1–1000).

Overbridge-based 3D micromixers connect 3D structures together using a bridge-shaped channel. Their mixing mechanism is mainly based on the concept of splitting and recombining. In order to conceptualize cancer cells, Yang et al. [88] proposed a three-dimensional Tesla structure. They built their micromixer by stacking Tesla structures on top of one another, and their experimental and numerical studies revealed that it achieved high mixing for Reynolds values between 0.1 and 100.

A variety of designs are proposed for 2D micromixers as well. T-Type and Y-Type mixer structures are known as the preliminary designs for 2D micromixers. These designs suggest very low mixing efficiency. Therefore, various techniques and approaches are reported to enhance their performance. The working principle of these methods has been categorized differently in literature [75], [76], [89]. Here, it is tried only to represent several of the prominent ones, although the combination of these methods has been implemented recently, thus making it difficult to classify each design exclusively to one category.

Convergence-divergence structure is one approach. This structure increases the contact area between the fluids, which improves mixing efficiency, and generates expansion vortices, which disrupt the laminar flow in microchannels. By using two geometrical forms, namely raccoon and serpentine, Mondal et al. [90] numerically examined the performance of wavy micromixers in various flow regimes. Their findings showed that the mixing index increased with the wavelength structure of their designs; however, the raccoon design's mixing performance was superior to the serpentine one for the given Reynolds number despite having a higher pressure drop.

Another technique that attracted a large number of scientists was the use of curved or spiral-based micromixers. Centrifugal forces created dean vortices in the curved channels. This way, the mixture's efficiency will improve as more loops are added. These structures are also simple to combine with others to improve mixing performance. One of the most notable features of curved micromixers is their efficiency at high Reynolds numbers. An intriguing double spiral-based micromixer with several mixing sections was proposed by Sudarsan and Ugaz [91]. A central S-section connected the spiral microchannels. They investigated five distinct spiral arrangements and found that the Dean flows helped them achieve a 0.9 mixing efficiency in the middle of the second segment.

Another strategy for improving mixing in basic T-Type and Y-Type mixers is to generate vortices and chaotic advection by introducing obstacles. Most obstacle-based micromixers include a variety of embedded grooves or barriers of varying shapes and heights to facilitate mixing. Obstacles can be built on the walls or inside the microchannels. Many numerical and experimental studies have examined the mixing process by utilizing various configurations of obstacles or by combining them with other methods. The passive micromixer fabricated by Wang et al. [92] has been shown to have high mixing efficiency for Reynolds numbers between 0.1 and 500. The micromixer is made up of 64 groups of triangle barriers. Both simulation and experimental data indicated that larger apical angles and more groups of triangular barriers resulted in higher mixing efficiency.

Several more active and passive mixer designs have been explored numerically or experimentally in the literature. To summarize, the architecture of active micromixers is typically not overly complicated, and the mixers are much simpler to operate. However, since they are

dependent on external energy sources, their operation is costly, and it is more challenging to integrate them with the other microfluidic components [93].

Passive micromixers, on the other hand, do not require any external equipment or power sources other than to pump fluids. The mixing is carried out via molecular diffusion and chaotic advection in passive micromixers, which exclusively rely on the unique geometry of the channels rather than on any external energy source. In conclusion, passive micromixers provide numerous advantages over active ones, including lower cost, portability, ease of use, and the potential for integration with Lab-on-a-chip devices. It should be noted that making three-dimensional passive micromixers needs intricate manufacturing procedures [94].

Simple fabrication, low-cost operation, and compact design while having high mixing efficiency were the main objectives considered for our micromixer. Based on the studies made in the literature, several designs are fabricated and experimentally analyzed to fulfill the desired goal. In the next section, detailed information about these designs is discussed.

4.2 Design

Aiming for a low-cost operation system is highly favorable in the proposed device. Cutting down the additional equipment is vital for making the device economical. It increases the device's chance of being portable, thus, closer to the idea of a fully lab-on-a-chip device. As explained, active micromixers are not an appropriate candidate due to their external energy source requirement leaning us toward using passive micromixers. Three-dimensional passive micromixers challenge the simple fabrication goal, which in turn makes the disposability of the device difficult to achieve. Two-dimensional passive micromixers would have been the most appropriate choice according to the proposed goals [20], [94].

Mixing techniques often rely on producing chaotic advection at the microscale, where the fluid motion is erratic, and hence pressure and velocity fluctuate randomly in space and time. Molecular diffusion, along with chaotic advection, is essential for mass transfer in micromixers. Species mixing is primarily due to molecular diffusion between layers of different concentrations in flow regimes where the flow is strictly laminar [95], [96].

The folding, stretching, and splitting of the streams caused by disturbing the flow is what makes chaotic advection so efficient at low Reynolds numbers. The process of mixing through diffusion would take an excessive amount of time and require an extremely lengthy channel. Increasing the contact area between the fluids to be mixed is necessary to hasten the process. Furthermore, due to the small volume of target DNA that must be amplified, a micromixer with high efficiency at low flow rates is preferred [74].

Given the adequate understanding of crucial factors in the mixing performance of two-dimensional passive micromixers, several designs were fabricated and analyzed to find the most convenient for our application. Each design underwent modifications to boost the chaotic advection and molecular diffusion by changing the length and width of the channel, shape and location of the grooves, as well as their dimensions. The characteristics of the designs given here are the same as the ones analyzed in the results section.

Design 1: Curved with barriers

As discussed earlier, curved-based micromixers are popular structures in micromixers. These structures can be easily combined with other methods to improve their performance. Gidde, R. & Pawar, P. [97] reported a significantly high mixing index (above 0.99) by incorporating obstacles on the walls of a wavy channel. The first design is inspired by their work due to its high

efficiency and uncomplicated structure to fabricate. The length of the channel is around 25 mm. Figure 22 demonstrates design 1 with its dimensions.

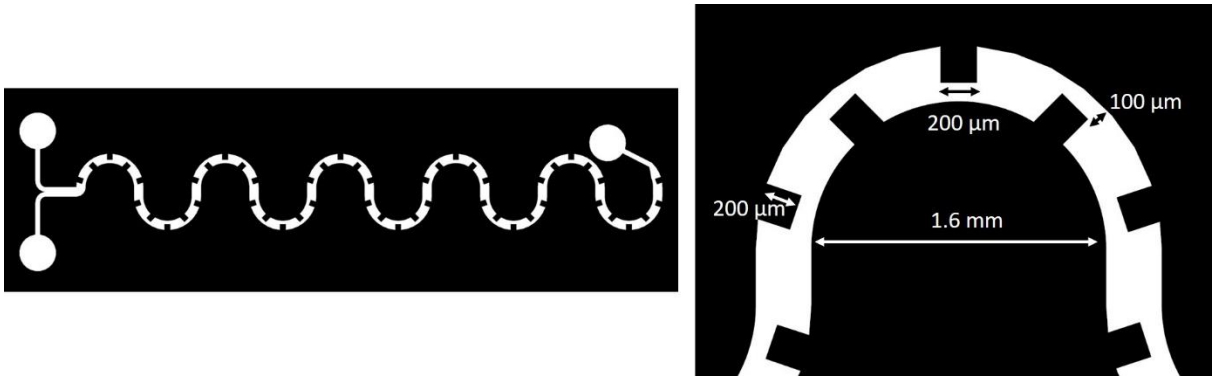

Figure 22 - Design 1 schematic and dimensions

Design 2: Zigzag

Zigzag designs are simple structures that stir the flow inside the microchannels. Figure 23 shows the detailed dimensions of this design. Sharp edges are added inside the channel to act as obstacles to improve the mixing quality. The length of the channel is around 60 mm.

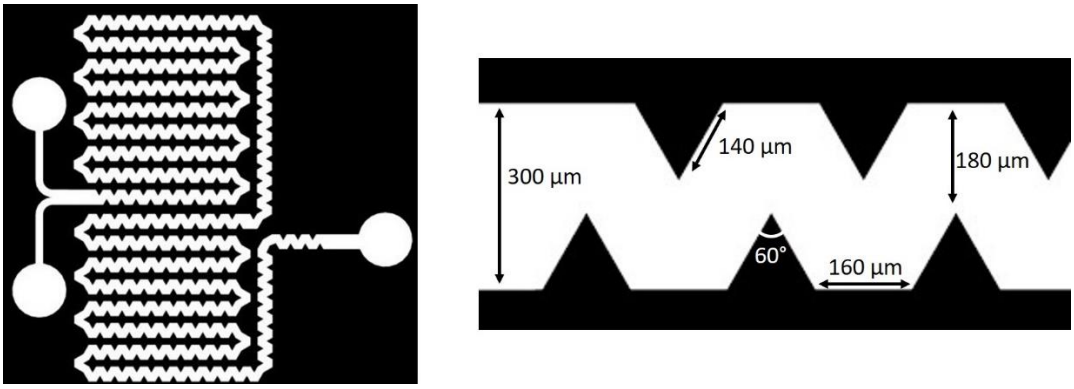

Figure 23 - Design 2 schematic and dimensions

Design 3: Serpentine

The serpentine design is inspired by the work carried out by Karthikeyan, K. & Sujatha, L. [98]. They suggested that their design is suitable for applications requiring small input energy and

a low flow rate. A few modifications were made to their design, and the detailed dimensions are shown in Figure 24. The overall length of this design is around 80 mm.

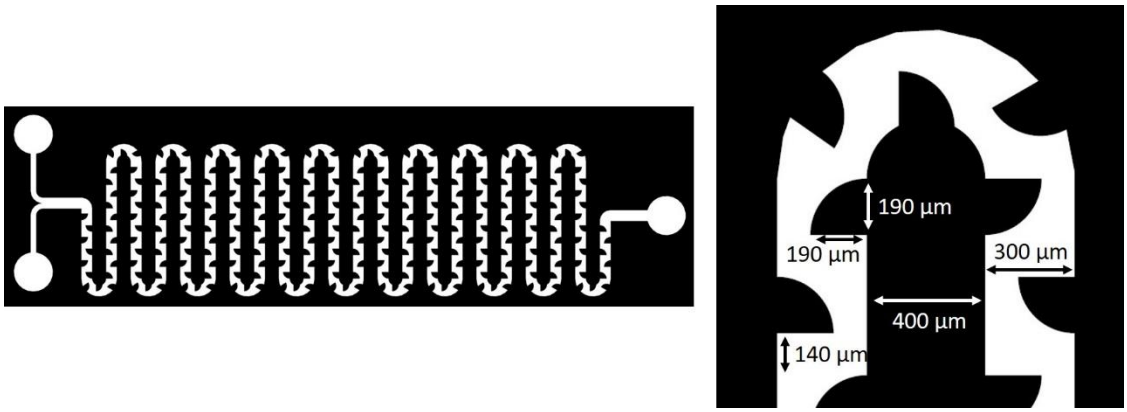

Figure 24 - Design 3 schematic and dimensions

4.3 Fabrication

Micromixer is made using soft photolithography. Negative photoresist SU-8 2075 (MicroChem, MA, USA) was used to fabricate the master for replica molding. A 3-inch silicon wafer was first cleaned using isopropanol (IPA). The photoresist was spin-coated on the wafer at a speed of 500 rpm for 10s followed by a speed of 2100 rpm for 30s to create approximately 100 µm channels (several other channel heights were also fabricated using the appropriate instruction). The wafer was then put onto a hot plate for 5 minutes at 65°C and 15 minutes at 95°C to perform the soft baking process. The mixer pattern was exposed onto the wafer by UV light (365 nm and 20 mW/cm^2) with a mask aligner for 13s. Post-exposure baking processes were performed at 65°C and 95°C for 4 and 10 minutes, respectively. Then, the wafer was developed in SU-8 developer for around 8 minutes, washed with isopropanol (IPA), and dried with nitrogen gas.

For the last step of fabricating the mold master, the wafer underwent hard baking process for 5 minutes at 150°C.

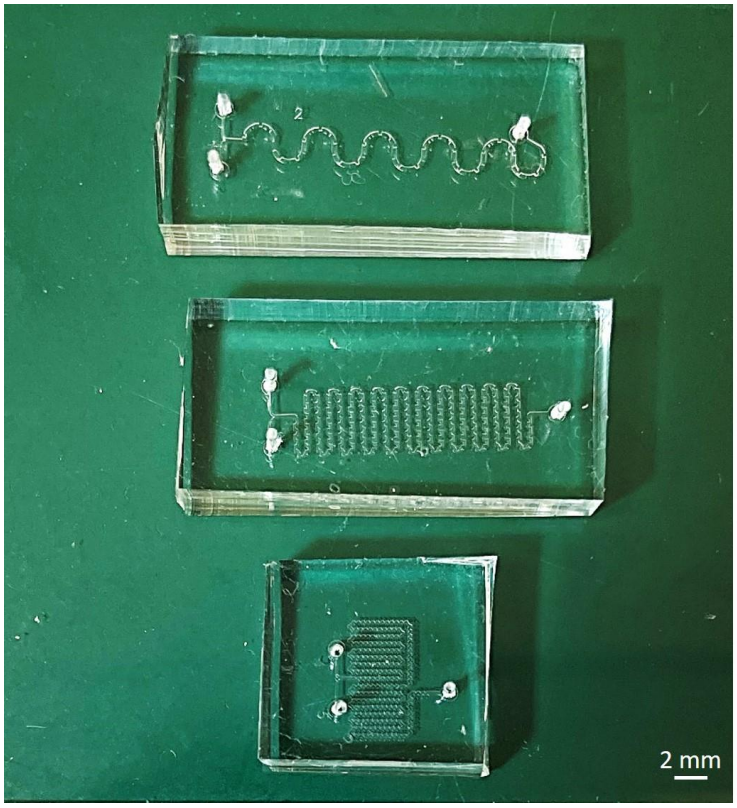

Figure 25 - Fabricated micromixers

After the preparation of the molds, liquid Sylgard 184 resin (Dow Inc., MI, USA) was stirred thoroughly with a curing agent in a weight volume ratio of 10:1. A specific amount of the mixture was poured onto the mold to form a 2mm structure. The mixture was kept in a vacuum chamber for 30 minutes to eliminate air bubbles. After curing the mixture for 2 hours at 80°C, the PDMS was gently peeled off from the mold, cut down to the same size as the reaction well block (2×1.5 cm), and fluidic access points were punched. At this stage, the mixer block was bonded to another PDMS layer using Oxygen plasma to be explicitly analyzed. However, in the integrated

device, the reaction well and micromixer blocks were bonded together. Figure 25 shows the three mixer designs fabricated by soft photolithography.

4.4 Experimental characteristic

4.4.1 Performance evaluation

A crucial aspect of a micromixer is its mixing efficiency which drastically improves detection sensitivity and speeds up the analysis time [66]. In this study, the mixing index is calculated by comparing the standard deviation of the pixel intensity of the desired point to that in the entirely unmixed section (inlet) [92]. This specific formula was picked over the others because studies have demonstrated that it is least impacted by lighting [99]. Figure 26 demonstrates the process of calculating the mixing index.

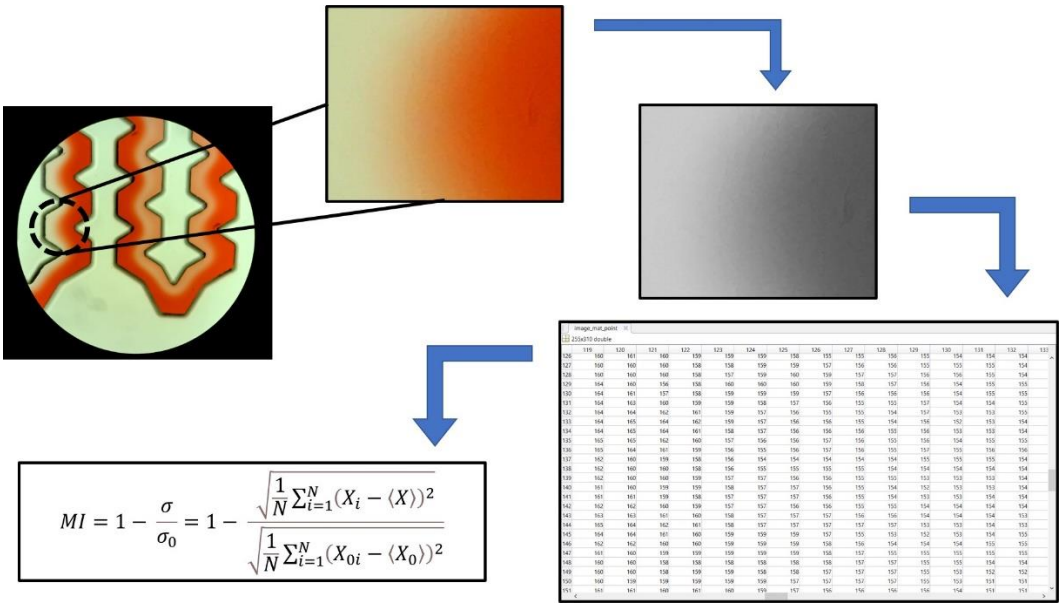

$$MI = 1 - \frac{\sigma}{\sigma_0} = 1 - \frac{\sqrt{\frac{1}{N}\sum_{i=1}^{N}(X_i - \langle X \rangle)^2}}{\sqrt{\frac{1}{N}\sum_{i=1}^{N}(X_{0i} - \langle X_0 \rangle)^2}}$$

Figure 26 – Mixing index calculation steps

To determine the standard deviation, pure water was injected from one inlet and a colorful stream from another one. The ECHO Revolution microscope took RGB Images from the desired region inside the micromixer channel. These images were then converted to greyscale values via homemade code in computer software. These values range from 0 to 255, corresponding to the intensity of each pixel in the original image. The values were then normalized according to the maximum intensity, resulting in normalized values X_i which range from 0 to 1. The mixing index is then expressed by:

$$MI = 1 - \frac{\sigma}{\sigma_0} = 1 - \frac{\sqrt{\frac{1}{N}\sum_{i=1}^{N}(X_i - \langle X \rangle)^2}}{\sqrt{\frac{1}{N}\sum_{i=1}^{N}(X_{0i} - \langle X_0 \rangle)^2}} \quad (1)$$

Where, $\langle X \rangle$ denotes the average value over the normalized values, and N is the number of data. Standard deviation at the non-mixing section (σ_0) would be equal to 0.5 if the flow rates are similar at the inlet, implying completely segregated streams.

4.4.2 Experimental setup

Two fluid streams were flowed through the mixer using a syringe pump (Cole-Parmer dual syringe pump) and two glass syringes of 500 µL size (HAMILTON Gastight syringe, 1700 series) to investigate the mixing performance. One of the syringes was filled with pure DI water, and the other was filled with diluted food color. The experimental apparatus is shown in Figure 27, where the mixing performance was observed and captured by the microscope and evaluated using equation 1.

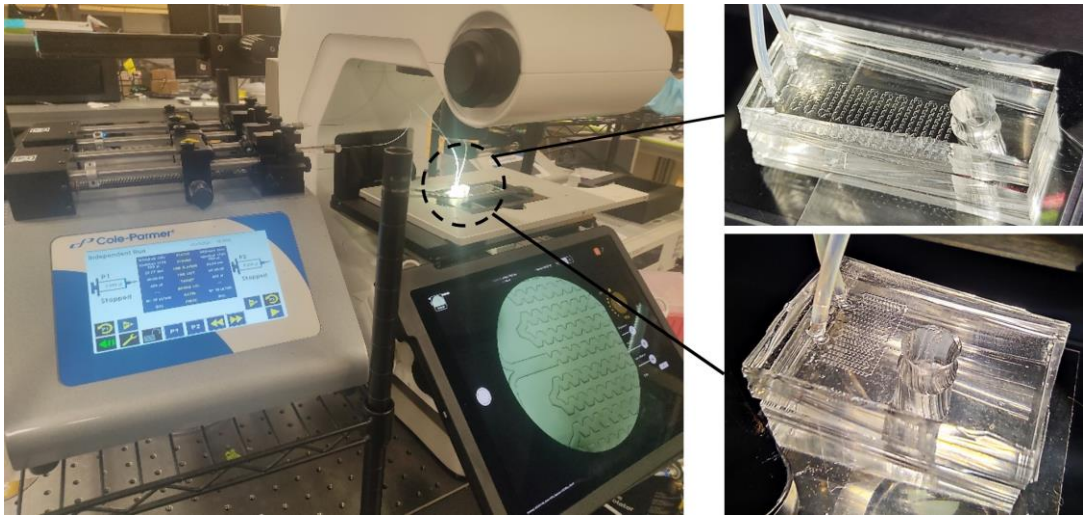

Figure 27 – Experimental setup for evaluating micromixers

The flow velocity is crucial in the performance of the mixer as it corresponds to the Reynolds number. Reynolds number represents the ratio of the fluid momentum to the viscous friction force, and is defined as:

$$\mathrm{Re} = \frac{\rho U D_h}{\mu} \qquad (2)$$

ρ is the fluid density ($kg \cdot m^{-3}$), U is the fluid velocity ($m \cdot s^{-1}$), D_h is the hydraulic diameter (m), and μ is the dynamic viscosity ($kg \cdot m^{-1} \cdot s^{-1}$) of the fluid. Tests were conducted with total flow rates in the range of 0.5 to 50 $\mu L.min^{-1}$. Mixers with different channel heights were also fabricated and analyzed.

Another factor that governs the flow characteristics is Peclet number which is defined as the ratio between the advective transport and the mass transport via diffusion.

$$\mathrm{Pe} = \frac{UL}{D} \qquad (3)$$

where L is the characteristic length, and D is the diffusion coefficient. The diffusion coefficient used in our experiments is $D = 4.9 \times 10^{-9}\ m^2.s^{-1}$ [100].

Instead of using PTFE Luer locks for syringes (Figure 28a), a combination of needles and disposable tubes was used. Implementing this method reduces the chance of sample-to-sample cross-contamination since new tubes will be employed for each test. The tests for evaluating the efficiency using a colorful stream were also conducted by this method to ensure the actual amplification test would be performed under the same conditions.

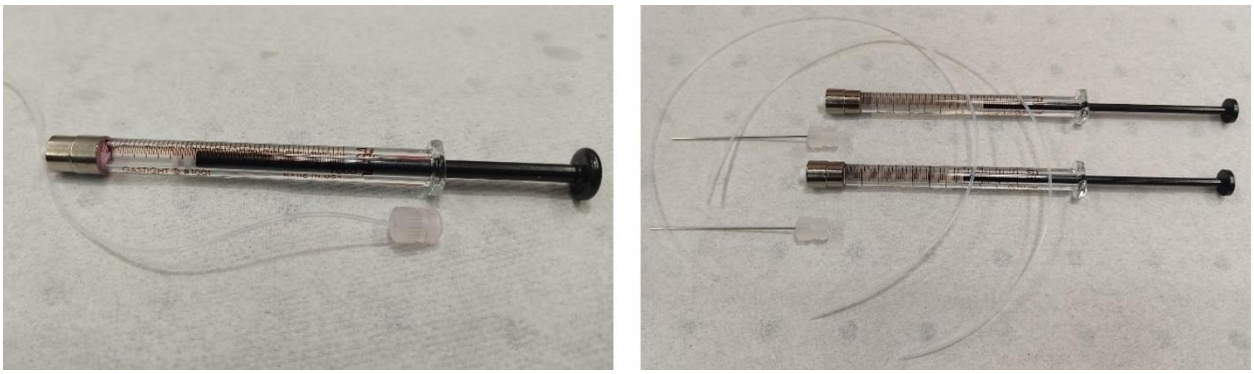

(a) **(b)**

Figure 28 – Syringes used for experiments. (a) PTFE Luer lock, and (b) syringe needles and disposable tubes

4.5 Results and discussion

A series of experiments were conducted to select the most appropriate micromixer design. After each experiment, designs with low efficiencies were dropped out. Sometimes, the size and position of obstacles and the length of the micromixer were also modified. Preliminary experiments were done under equal flow rates in inlets. The first set of experiments aimed to determine the appropriate channel height, and then the flow rate was decided. After deciding these parameters and narrowing down the mixer design to the appropriate one, the flow rate ratio was set to the target DNA and PCR mixture ratio.

4.5.1 Channel height

Molecular diffusion considerably assists mixing quality in low Reynolds numbers. Increasing channel height would increase the contact surface between the streaming flows resulting in higher molecular diffusion, while lower channel heights are much easier to fabricate. Micromixers were fabricated at three heights of 40 µm, 100 µm, and 180 µm to investigate the effect of channel heights. The total flow rate was fixed at specific amounts in the range of 0.5 to 50 µL.min^{-1} to simultaneously monitor the performance of mixers as well. To compare the mixing quality of the mixers the microscope images were used as shown in Figure 29.

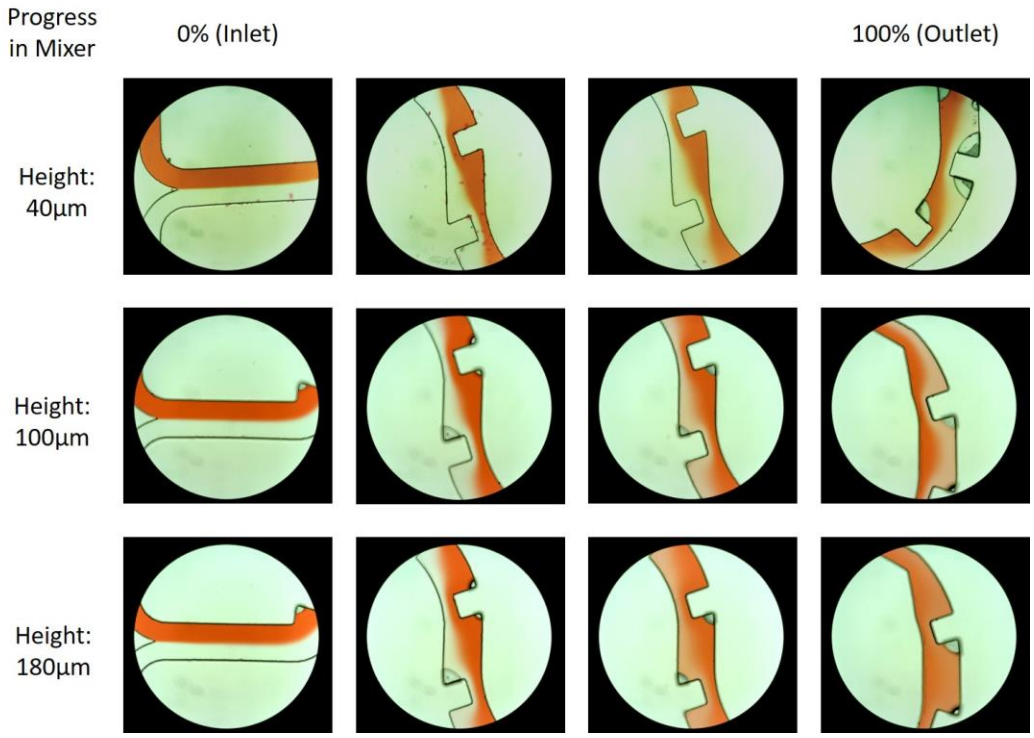

(a)

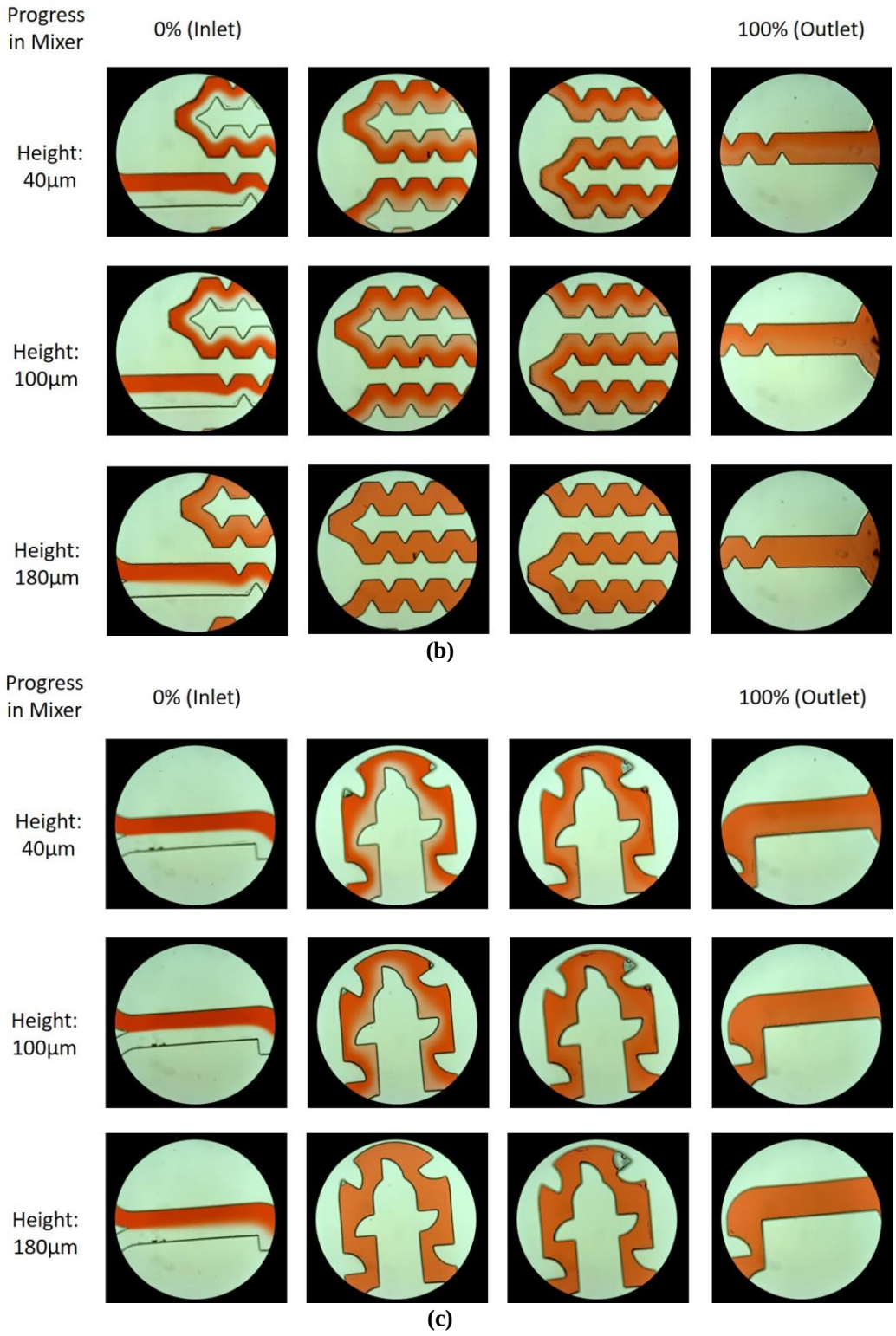

Figure 29 - Performance of mixers in different channel heights and total flow rate of 20 µL.min^{-1}. (a) design 1, (b) design 2, (c) design 3.

Figure 29 presents the performance of three mixer designs under total flow rate of 20 $\mu L.min^{-1}$. (10 $m.s^{-1}$ from each inlet). Images located in a row are representatives of a specific channel height. These images were captured at different locations along the channel at equal distances, starting from the inlet as the first image on the left of each row. The flow direction is from left to right. The corresponding Reynolds number for heights of 40 µm, 100 µm, and 180 µm is 2, 1.66, and 1.39, respectively. The calculated Peclet numbers for these heights are 4000, 3400, and 2830, respectively as well. Evidently, the quality of mixing increases as we move along the channel. At low Reynolds numbers, molecular diffusion prevails in the mixing mechanism of two streams. Therefore, the time the working fluid stays in the micromixer greatly influences the mixing quality. The longer the channel, the higher the mixing quality will be.

As expected, increasing channel height showed noticeable effect on mixing quality in all designs. As the height increases, the contact area between the two working fluids grows as well. By fixing the flow rate at a constant value, the flow velocity inside channels decreases as well. Thus, the streams will have more time to diffuse at a constant length. In other words, the fluid-fluid interaction time increases by increasing channel height, and the diffusion rate also grows. The change in Peclet number also approves the influence of increasing channel height. As the channel height increases, the Peclet number starts to drop. With the decrease in the value of Peclet number, the rate of molecular diffusion grows contributing to a higher mixing quality. The effect of height is clearly visible in the second images of design 2 and design 3 in Figure 29, while calculating the mixing index is needed to compare the performance at the outlet due to the high level of mixing.

Design 1, on the other hand, does not show efficient mixing, as illustrated in Figure 29a, especially in comparison to the other two designs. It is important to note that the channel length in

design 1 is shorter than the others. This design requires a more extended channel as the effect of increasing height becomes noticeable after the working fluids progress through more than half of the mixer. A similar design with a channel height of 0.4 mm was reported to have significantly high efficiency (0.97 efficiency at Re= 5) [97] while the maximum efficiency achieved in our experiments was 81.46 percent. In addition to the difference in channel height, other reasons can also explain this poor performance. The performance of the mixer was evaluated using numerical simulation, which is ideal, while in our set of experimental tests, lots of bubbles were formed around the obstacles. As a result, obstacles were unable to change the flow pattern and stir the fluids. Some modifications were also made to the size and shape of the obstacles as well as the curve of the channel. However, the other two designs still presented better performance.

To better understand and compare the mixing quality, Figure 30 shows the mixing efficiency of the mixers at total flow rate of 20 µL.min^{-1} using equation 1.

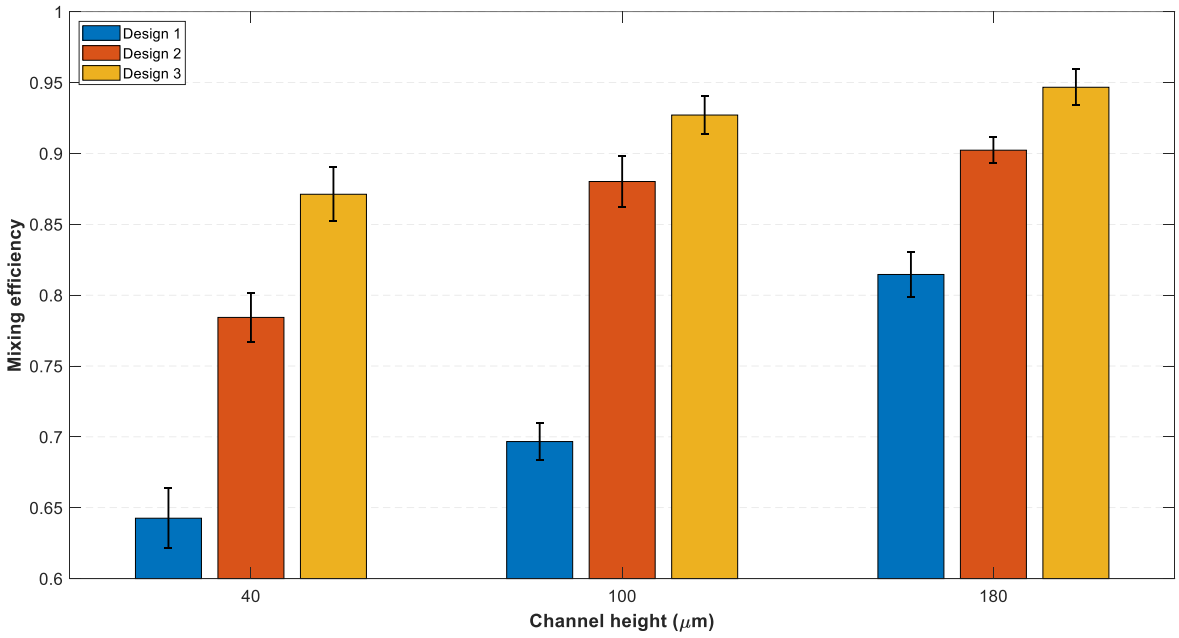

Figure 30 - Mixing efficiency of mixers at total flow rate of 20 µL.min^{-1} and different channel heights

None of the mixers show satisfactory results in a channel height of 40 µm. Flows require more time for mixing, which is undesirable given that it would remarkably lengthen the channel. It should be noted that as efficiency rises, increasing it becomes more and more challenging. The improvement in mixing quality from the height of 100 µm to 180 µm is not as significant as it is from 40 µm to 100 µm. From the practical view, channels with high heights are hard to fabricate. Also, the molds are more susceptible to getting deformed due to their high aspect ratio. Although the height of 180 µm has higher mixing efficiency, 100 µm channels provided satisfactory results to be considered as the appropriate option for the mixer.

Experimental tests were conducted at other flow rates as well, and the mixers followed the same trend. Design 1 had the worst performance, and design 2 and design 3 suggested close mixing efficiencies, especially in small flow rates. Moreover, as the flow rate decreases, the difference between the efficiencies of channels with heights of 100 µm and 180 µm decreases. According to Figure 30, the mixing efficiencies of design 2 and design 3 are 0.88 and 0.92, respectively, at the height of 100 µm and total flow rate of 20 $\mu L.min^{-1}$. In the upcoming sections, the minimum efficiency required for PCR amplification is also discussed. In the next section, the effect of flow rate on efficiency is investigated.

4.5.2 Total flow rate

At high Reynolds numbers (Re>10), convection plays a key role in mixing, and the mixing efficiency increases by increasing the Reynolds number. As inertial forces increase, advection rises as well, which disturbs the flow field and promotes mixing by creating a disturbance in the flow field [97]. However, achieving this Reynolds number requires very high flow rates, which has several disadvantages. Namely, the sample consumption rate will increase and make experiments expensive. It can also damage the bonding layer and waste the samples due to leakage.

Consequently, high flow rates were not studied for our device. It is also worth mentioning that micromixers at low Reynolds numbers (Re<1) exhibited excellent performance [92], [97].

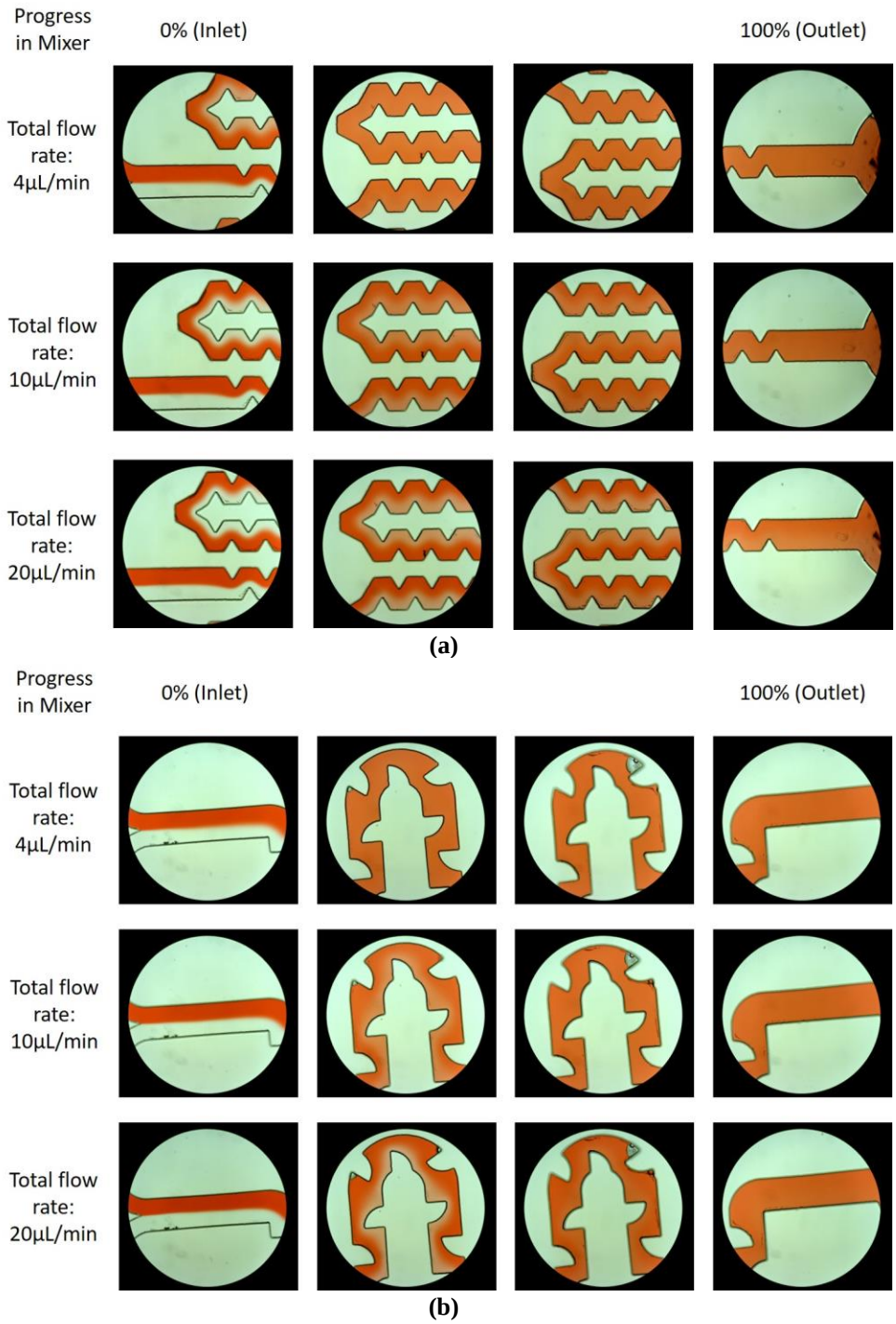

Figure 31 - Performance of mixers in different flow rates and channel height of 100 µm. (a) design 2, (b) design 3

At this Reynolds, diffusional mass transfer is the main mechanism for mixing. To find the appropriate flow rate for our device, experiments were conducted at total flow rates of 0.5, 1, 4, 10, 20, and 50 $\mu L.min^{-1}$. The images captured at total flow rates of 4, 10, and 20 $\mu L.min^{-1}$ are shown in Figure 31. Since design 1 demonstrated poor performance, only results from design 2 and design 3 are included in this part.

Figure 31 presents the microscopic images of design 2 and design 3 at a channel height of 100 μm. The images in each row represent a specific flow rate. The corresponding Reynolds number for flow rates of 4, 10, and 20 $\mu L.min^{-1}$ are 0.33, 0.83, and 1.66, respectively. Peclet number is evaluated as 680, 1700, and 3400, respectively for these flow rates. The adverse effect of increasing the flow rate on mixing quality is evident, especially by observing the second images of each design in Figure 31. As the flow rate increases, working fluids are driven toward the outlet without having sufficient time to interact. As a result, the flow must travel a longer distance to achieve similar mixing efficiency. Moreover, the increase in total flow rate would increase the Peclet number implying that the molecular diffusion is decreasing which results in a drop in mixing efficiency. However, both designs suggested high efficiencies at this height at the outlet, making the comparison rather difficult without mixing index calculations. Therefore, the bar chart in Figure 32 is presented to better understand the effect of total flow rate on efficiency. Total flow rate of 20 $\mu L.min^{-1}$ showed poor performance in comparison to other flow rates. In addition to poor performance, a high flow rate might damage the bonding and result in a waste of PCR mixture. Handling low target DNA volume (3 μL) can also be difficult. Therefore, it was decided not to choose a total flow rate of 20 $\mu L.min^{-1}$ and higher. Both total flow rates of 10 and 4 $\mu L.min^{-1}$ suggested satisfactory results. However, mixing at total flow rate of 4 $\mu L.min^{-1}$ and lower takes

too much time. Since the mixing efficiency of total flow rate at 10 µL.min^{-1} is sufficient for our application, we decided to choose this flow rate over flow rate of 4 µL.min^{-1}.

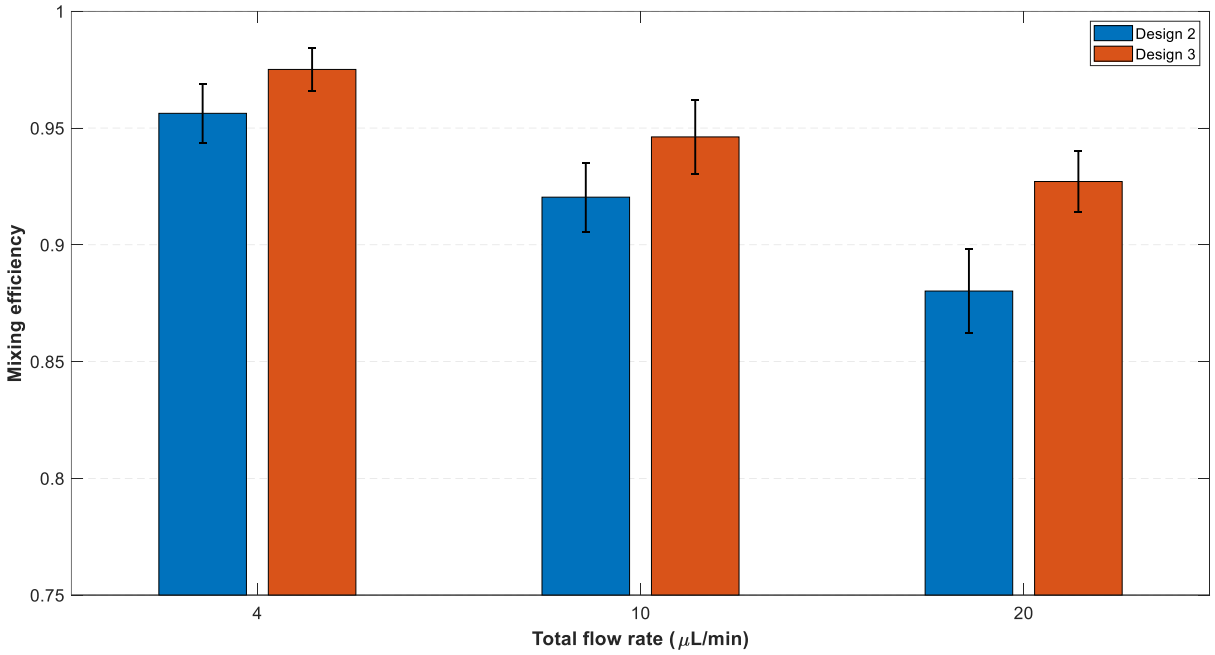

Figure 32 - Mixing efficiency of mixers at a channel height of 100 µm and different total flow rates

Design 3 displayed better performance over design 2 similar to the previous section. This can be explained with the chaotic flow regime created by the high number of grooves across its channel walls. Although design 3 achieved better mixing efficiency, design 2 is compact and more convenient for our small disposable device. Unlike design 2, design 3 occupies a larger space making its production costly as it requires more material. Moreover, integrating a compact mixer with the reaction well is simpler. It should be noted that the mixing channel of design 3 is around 20 mm longer than design 2. According to the plot in Figure 33, they show a very close mixing index at a distance of 60 mm from the inlet, which is the total channel length of design 2.

Design 3 reaches high efficiencies much faster than design 2 due to its special obstacle-based geometry. However, it was not possible to make design 3 as compact as design 2, even by

reducing its length. Furthermore, bubbles were formed in several regions around the grooves, which can impact its performance or even block the channel, which never happened in any experiment using design 2. The next section will cover the selected mixer's performance with PCR flow rate ratio.

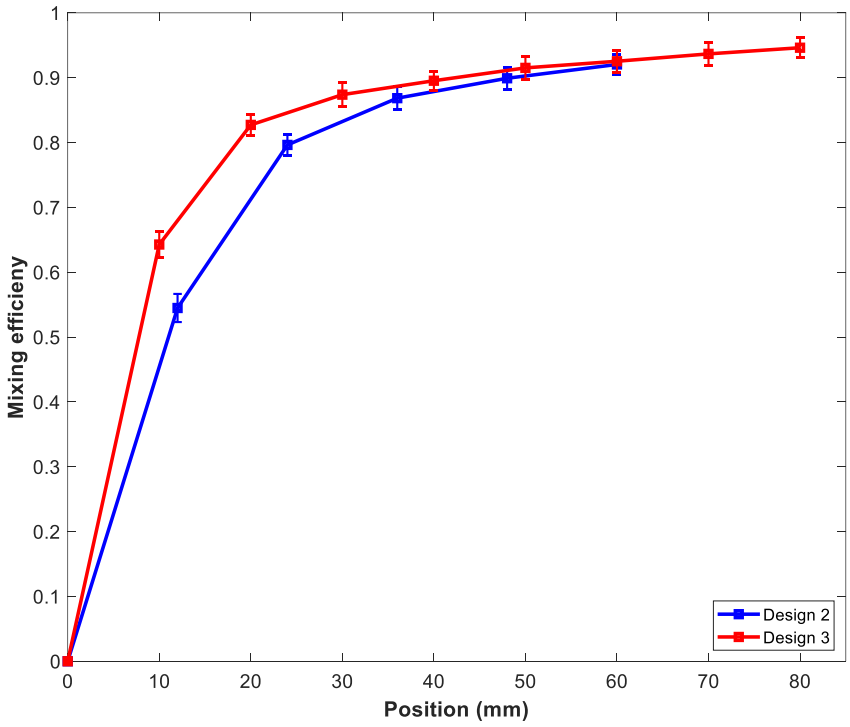

Figure 33 - Mixing performance comparison of design 2 and design 3 with respect to channel length

4.5.3 Mixer performance at PCR flow ratio

The channel height and the total flow rate of the micromixer were decided in previous sections. Design 2 demonstrated satisfactory performance under chosen conditions, and the issues with design 1 and design 3 were explained.

The preliminary tests were conducted at equal flow rates, while flow rates must be different for amplification tests. The volume ratio of the target DNA and master mix is 3:17. Therefore, the flow rates at the inlet should match with this volume ratio. Since total flow rate is decided to be

10 µL.min^{-1}, the flow rate at one of the inlets would be 1.5 µL.min^{-1} and 8.5 µL.min^{-1} in the other one. In this section, the performance of design 2 under this certain flow ratio is investigated. This experiment was also done using design 3, but bubbles were still forming throughout the channel. Figure 34 Shows an overview image of design 2 in a flow rate ratio of 8.5/1.5 µL.min^{-1}.

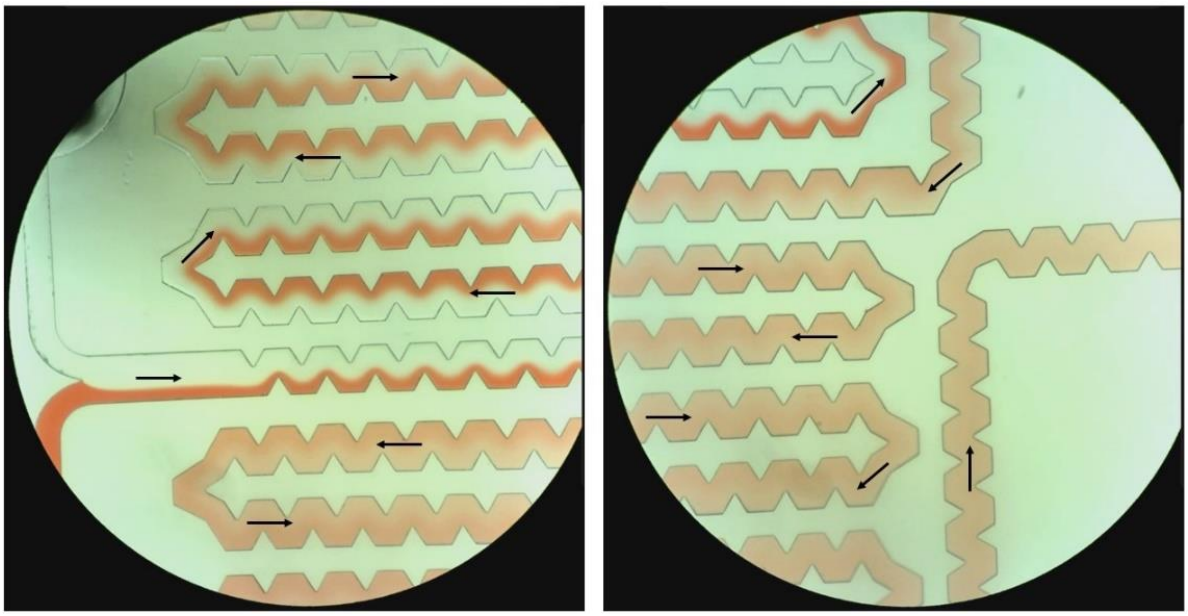

Figure 34 - Mixing performance of design 2 under flow rate ratio of 8.5/1.5 µL.min^{-1}

The continuous growth in mixing quality along the mixer is noticeable after the working fluids pass through each loop. The growth rate of mixing quality decreases as the mixing efficiency rises to high values. 80 percent mixing efficiency is surpassed after the flow reaches halfway through the mixer. To better understand the growth behavior, mixing indices were calculated.

Figure **35**a demonstrate mixing efficiencies at different regions throughout the mixer under flow rate ratio of 8.5/1.5 µL.min^{-1}.

The performance of both mixers (design 2 and design 3) with the flow rate ratio of PCR amplification was compared to the previous results of equal flow rates. The plots demonstrated

similar trends, although the values of mixing indices were barely changed. This is due to the fact that, unlike equal inlet flow rates, the standard deviation at the inlet was not equivalent to 0.5 resulting in an alteration of mixing efficiency values.

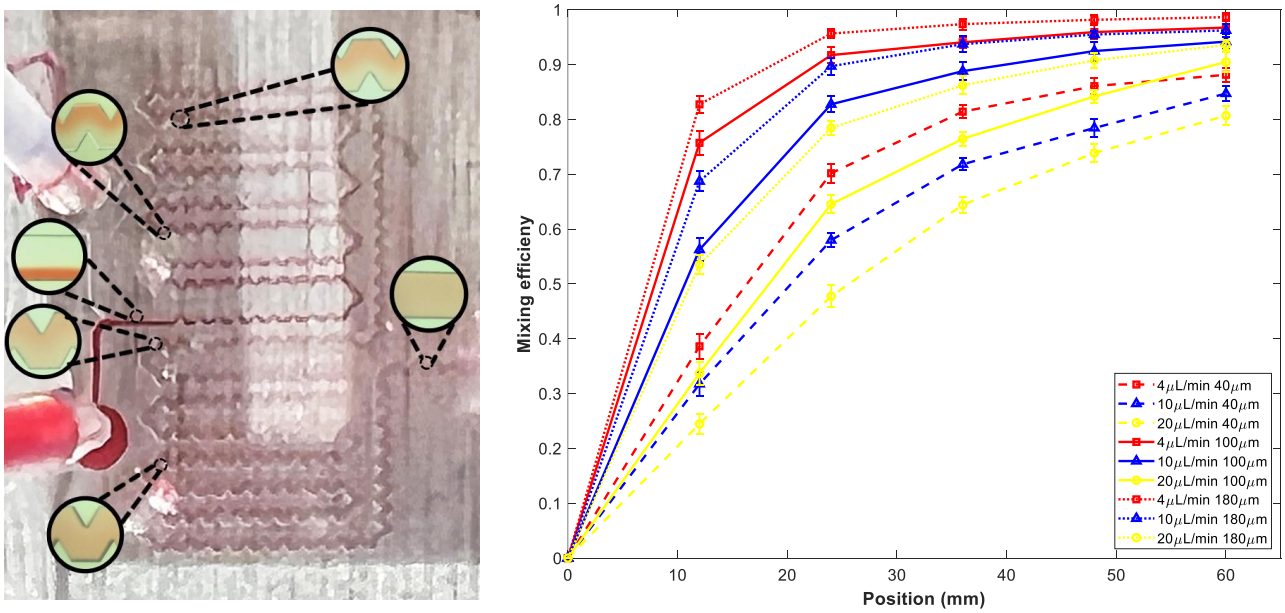

(a) **(b)**

Figure 35 – Micromixer performance at PCR flow ratio. (a) Microscope images throughout design 2, and (b) Performance of design 2 at 3 different total flow rates and 3 different channel heights

Figure **35**b illustrates plots for three different heights and three different total flow rates. The results are in great consistency with the ones achieved in previous sections. The regions used to calculate mixing indices are tried to have identical distances from each other. These regions with the corresponding microscope image are shown in

Figure 35a. The channel height of the mixer presented in this figure is 100 µm, and the total flow rate is 10 µL.min^{-1} which are final characteristics used for PCR amplification. The final efficiency with these characteristics is 94.17%.

4.5.4 Minimum mixing requirement for amplification

Several tests were carried out before choosing design 2 and the suggested characteristics to ensure PCR amplification will be performed successfully. These tests aimed to find the required mixing efficiency for DNA amplification. Experiments were performed under different flow rates and channel heights, as well as different mixer designs. For example, one design was fabricated half the length of design 2 but with the exact dimensions. It is complicated to report a mixing index as the minimum value required for successful amplification. It would be more practical to report the results in different efficiency ranges.

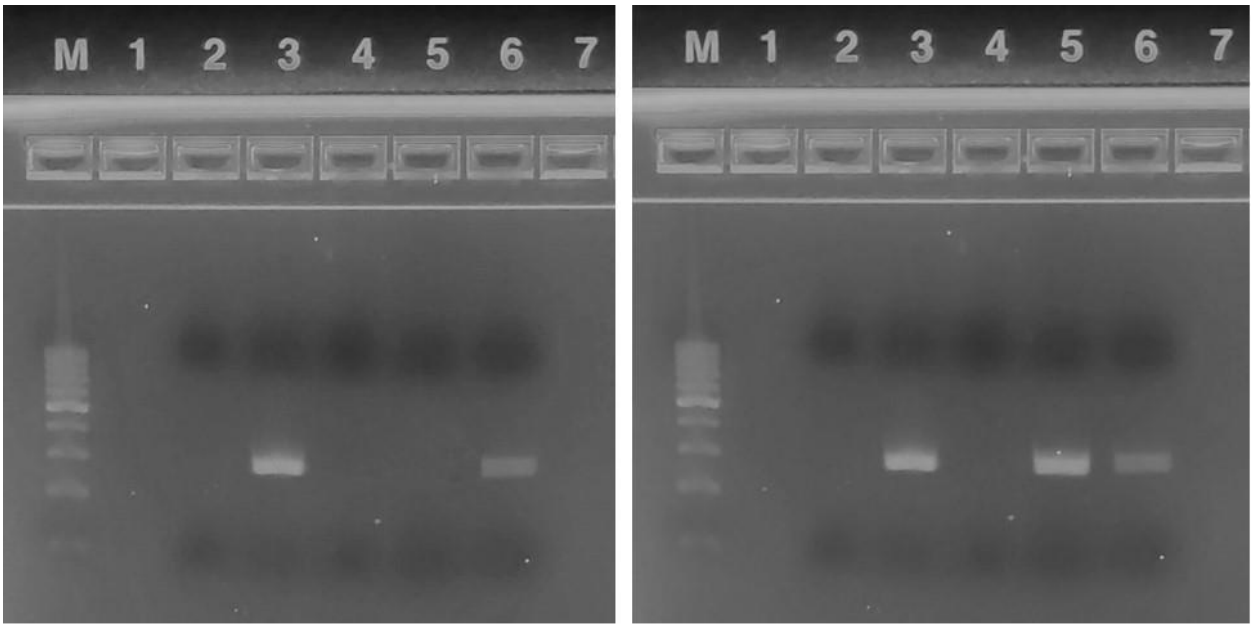

(a) **(b)**

Figure 36 - E-gel electrophoresis test results to find the minimum mixing efficiency requirement for DNA amplification. (a) efficiencies below 0.85, and (b) efficiencies between 0.85 and 0.9

Figure 36 presents E-gel electrophoresis results where lane 2 is negative control, lane 3 is positive control, lanes 4 to 6 are three different tests. We found that for efficiencies below 0.85, no amplification occurs or only unspecific bands appear. Figure 36a shows an example of

amplification results for efficiencies below 0.85. In Figure 36b, on the other hand, a band is formed. This figure is for efficiencies between 0.85 and 0.9. The problem with this region is that the results are not repetitive, and the brightness of bands is not always similar to the positive control, while in efficiencies above 0.9, results were satisfying. The next chapter discusses the integration of different parts of the device, and the final results are analyzed.

Chapter 5: Integrated device verification

5.1 Microfluidic chip integration

In previous chapters, PCR reaction well, microheater, temperature control system, and micromixer were analyzed. The design process was elaborated for each of these parts, and their performance was characterized. This chapter discusses the integration of these parts into a disposable compact lab-on-a-chip device. Finally, the performance of the device as a whole will be validated.

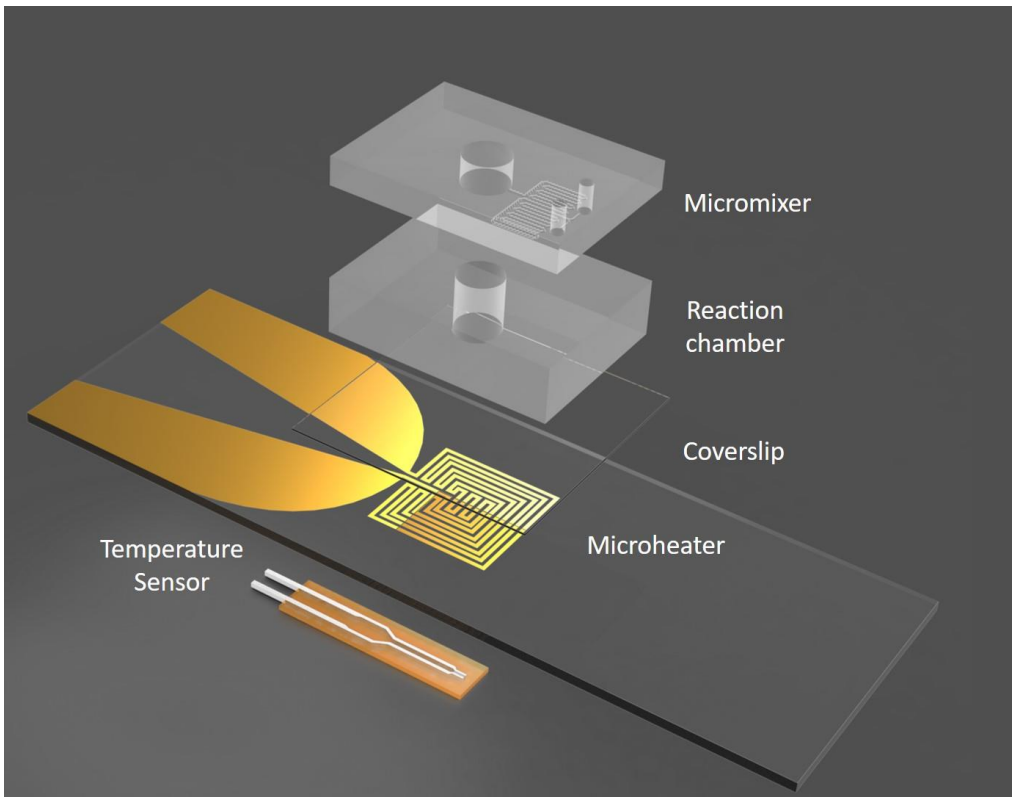

Figure 37 – Exploded view of the integrated device

Figure 37 represents an exploded view of the microfluidic device. Parts are fabricated separately and then assembled together. The micromixer, PCR well, and coverslip bond together

and form the disposable part of the device, while the heating and sensing parts are reusable after PCR amplification.

Figure 38 shows the integrated microfluidic device. To fabricate the disposable part, both reaction well block and micromixer block were exposed to oxygen plasma for 20s (Plasma Etch, PE-50, USA), brought into contact with each other, and incubated at 80°C for 2 hours to form an irreversible bond. The advantage of having a separate PDMS block for reaction well and bonding the micromixer on top of it is cutting out the need for a microvalve. Integrating microvalves into PCR microfluidic devices makes the fabrication process much more challenging, and supplementary equipment, such as an air compressor, is required for the valves to operate. Furthermore, since microvalves do not always perform ideally, some of the PCR mixture might flow back to the channels during the thermocycling process, resulting in wasting the mixture and lowering the quality of amplification.

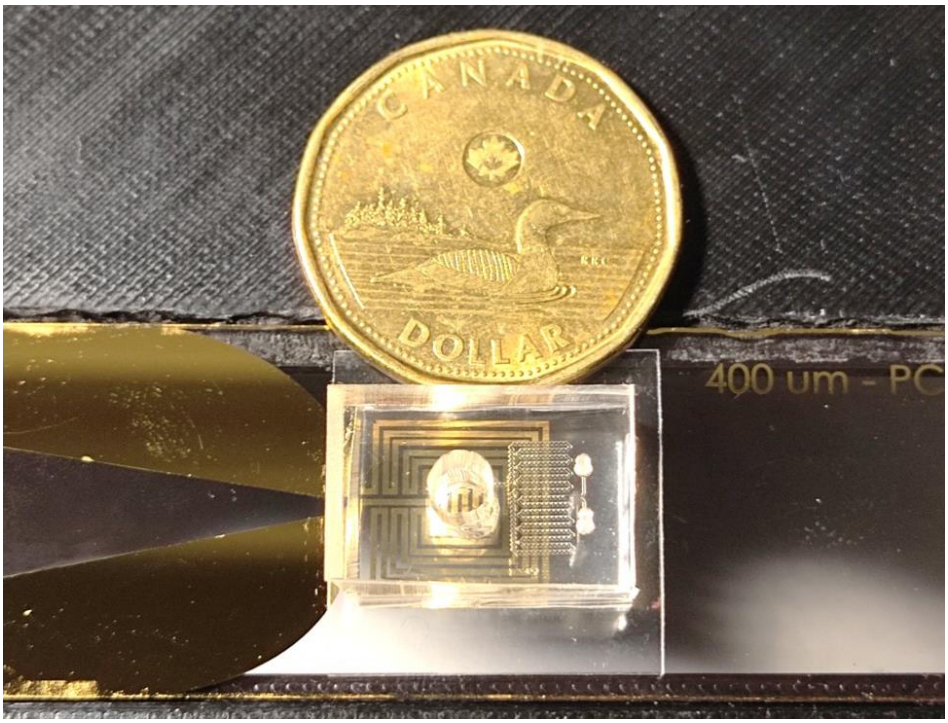

Figure 38 – Final fabricated integrated microfluidic device

The final stage of assembling the disposable part is bonding the block of the reaction well and micromixer to a coverslip (22 × 22 mm, Fisherbrand™) using oxygen plasma. This process thoroughly eliminates sample-to-sample contamination. Channels and reaction chambers in microfluidic devices, which lack disposability are often washed upon PCR completion. Therefore, reagents or washing liquids may be left in channels or absorbed by PDMS due to their porous structure leading to distortion in the next amplification process results. We were able to reuse the heating component of the chip for future amplifications, while the disposable section was simply replaced with a new one after each PCR cycle was finished, all thanks to the coverslip.

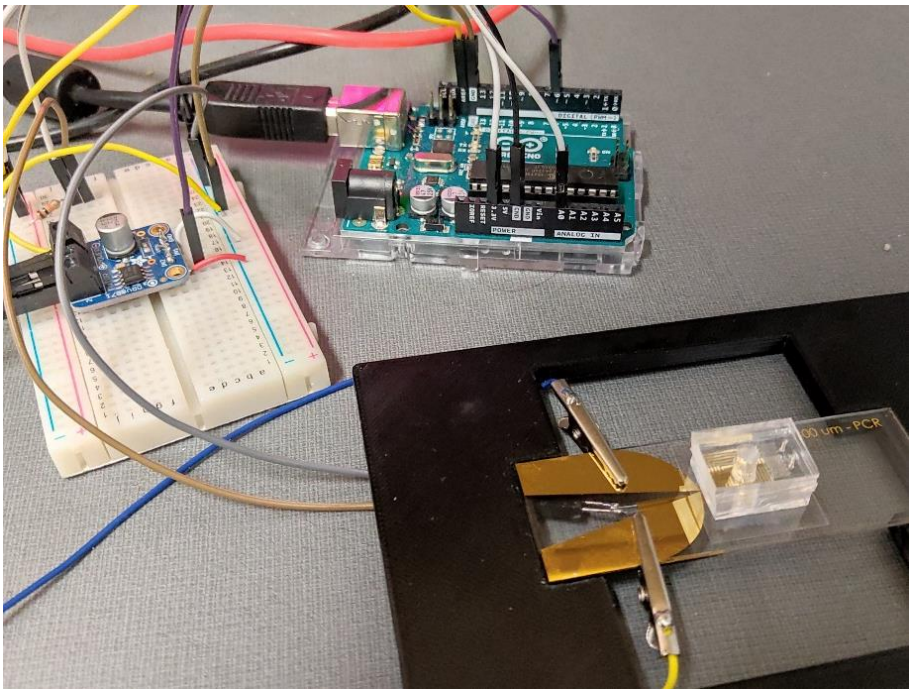

Figure 39 – Experimental setup of integrated device during PCR reaction

For conducting PCR amplification, the chip is first connected to the pump. 17 µL of the master mix was automatically mixed with 3 µL of 100-fold diluted λ-phage DNA through the micromixer and directly dispensed into the reaction well of the disposable block. The

Thermocycler automatically starts the PCR protocol monitored by the control system. The experimental setup is shown in Figure 39. After the protocol is finished, the amplified mixture is recovered for the post PCR process using E-gel electrophoresis.

5.2 Verification

5.2.1 Thermal cycling

The PCR thermal cycling was applied under the following protocol: First, to activate the Taq polymerase, pre-denaturation was done at 95°C for 5 minutes. Then, the PCR cycle was repeated 40 times: denaturation of the DNA template at 95°C for 15 s, annealing of primer at 54°C for 20 s, and extension of the DNA at 72°C for 20 s. The final step was elongation at 72°C for 1 minute. Figure 40 presents one of these cycles.

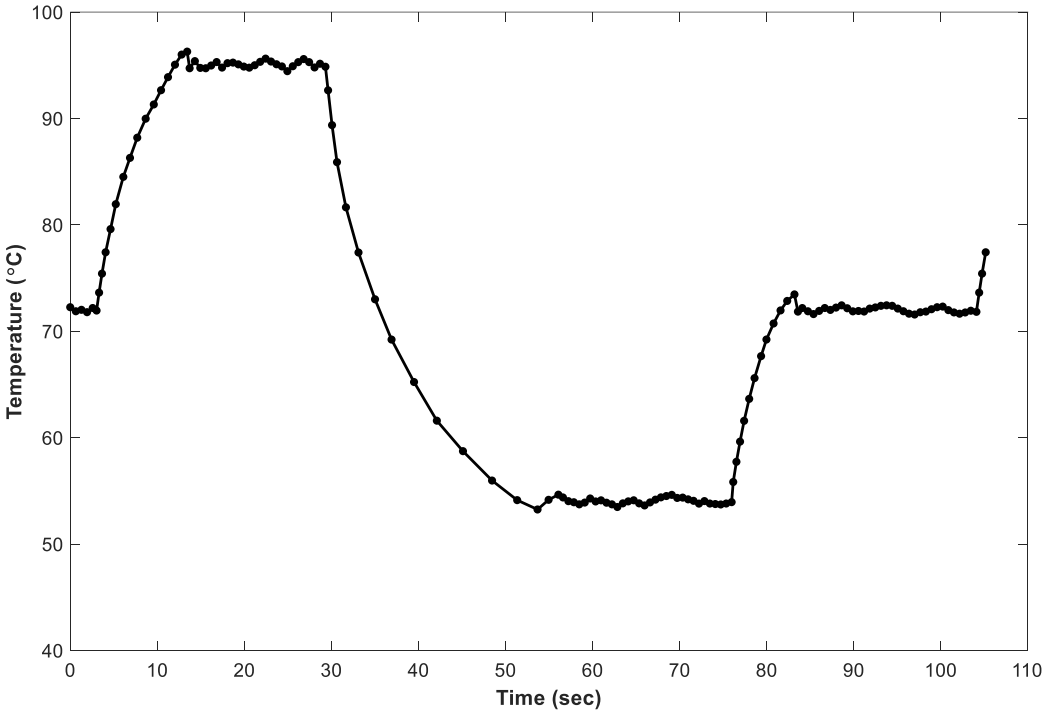

Figure 40 – One PCR cycle using the developed microfluidic device.

Each cycle was reported to take around 105 seconds. The average heating and cooling rate recorded was about 2.2°C/s and 1.7°C/s, respectively. The whole amplification takes between 70 and 75 minutes, while it was around 85 minutes for conventional PCR. In addition, the temperature was meticulously maintained at PCR step set points with a deviation of less than 1°C/s.

5.2.2 PCR reaction

To verify PCR amplification repeatability, three separate experiments were conducted using different lab-on-a-chip devices. The amplification performance of the device was verified by a conventional PCR referred to as λ DNA positive control. Figure 41 presents the final results visualized by E-gel electrophoresis.

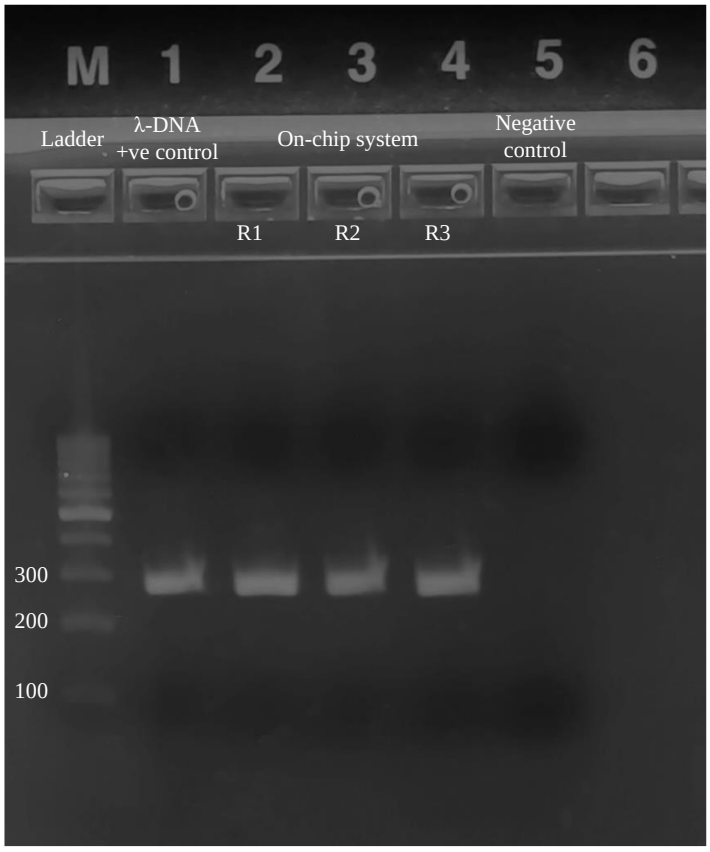

Figure 41 – E-gel results of the lab-on-a-chip device

Lane M is the 100-bp ladder DNA marker. Signal in Lane 1 is obtained by using the conventional PCR machine for positive control. Bands in lanes 2, 3, and 4 are the PCR products obtained by the lab-on-a-chip device. Lane 5 represents negative control.

The results demonstrate that this system can generate the correct amplified PCR base pair (300bp) and that degradation does not occur throughout the process. The brightness of bands can be used to qualitatively assess the efficiency of amplification. Since no significant difference in the PCR band intensities was observed, it can be interpreted that all parts performed efficiently.

Chapter 6: Final remarks

6.1 Conclusion

When diseases are in their early stages, the genetic material that causes the disease is only present in the infected human or animal in very low concentrations. This makes disease detection quite challenging. It is possible to increase the concentration of the agent by using a technique called PCR to multiply the agent's genetic material. Microfluidic PCR devices have a number of benefits over conventional thermal cyclers, including portability, reduced power/ reactants consumption, compact size, and improved temperature uniformity.

In this study, a disposable, compact, easy-to-fabricate, low-cost, and efficient lab-on-a-chip device is designed to amplify λ-DNA. The device is composed of several parts performing together to complete PCR amplification. Each of these parts was designed, fabricated, modified, and analyzed separately at first, considering the limitations of the whole device. Finally, the performance of the integrated device was analyzed.

Following are the steps that the integrated system takes to perform PCR: 17 µL of Master mix and 3 µL of the target DNA are mixed with high efficiency inside the micromixer. The resulting mixture is then streamed directly into the reaction well. The reaction well is located right above the microheater. Thermocycling is carried out by following the PCR protocol while the microcontroller unit monitors the temperature of the reaction well. The control system ensures uniform thermal distribution inside the reaction well. When thermocycling is completed, the amplified product is removed to analyze the performance of the lab-on-a-chip device compared to a commercial PCR machine using E-gel electrophoresis.

The PCR protocol consisted of pre-denaturation at 95 °C for 5 minutes followed by 40 cycles of denaturation at 95 °C for 15 s, annealing at 54 °C for 20 s, and extension at 72 °C for 20 s. The final step was elongation at 72 ◦C for 1 minute.

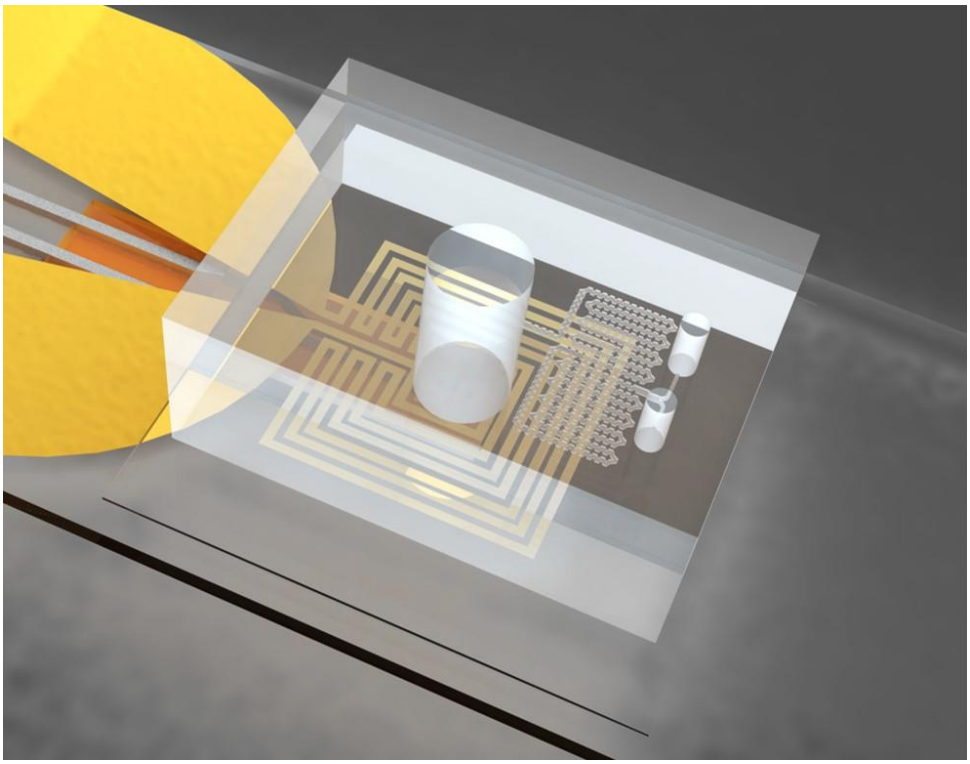

Figure 42 – Disposable Lab-on-a-chip device for PCR amplification

The reaction well is manufactured by punching a hole throughout a PDMS block. PDMS is biocompatible and does not degrade sensitive PCR reactants. The simple structure of the reaction well makes it convenient for mass production. Uniform thermal distribution of the mixture is crucial for efficient PCR amplification. Therefore, the diameter of the reaction chamber was decided to be 4 mm to make sure of thermal uniformity inside the well according to the comprehensive analysis made on microheater heat maps. In order to prevent evaporation, mineral oil covered the PCR mixture.

The microheater works by the joule heating principle. Heaters are made of gold electrodes patterned on glass slides via photolithography. The goal was to design a pattern with uniform temperature heat map and fast thermal response while consuming low power. Infrared thermal images and corresponding freeware analyzed the performance of the heaters. The selected microheater showed an average of 94.9°C in a circular area with a 4 mm diameter. Around 95% of the area was reported to have temperature uniformity with thermal variation <1°C protocol setpoints (54°C,72°C,95°C).

Thermistors were used as temperature sensors. The sensor was attached to the microheater's backside and calibrated to report the temperature of the mixture inside the reaction well. The control unit tunes the voltage to maintain the temperate based on the data from the sensor. The results showed that the control system could maintain the temperature with less than 1°C error at desired points. The average heating and cooling rates were about 2.2°C/s and 1.7°C/s.

Several designs were proposed for the micromixer. While most passive micromixers have complex structures and are difficult to fabricate, fabrication of the proposed design is not complicated using soft lithography. Molecular diffusion plays a dominant role in mixing quality in low Reynolds numbers. It was tried to increase diffusivity and chaotic advection by choosing curved structures and adding obstacles to the micromixer. The performance of micromixers was analyzed at different channel heights and total flow rates. The mixing efficiency was calculated by comparing the standard deviation of pixel intensity at desired point to the inlet. Channel height of 100 µm and total flow rate of 10 $\mu L.min^{-1}$ demonstrated most suitable results for our application. The selected micromixer reported mixing efficiency of 94.17% at chosen characteristics. It was also evaluated that no unspecific band will appear for efficiencies higher than 90% in E-gel electrophoresis.

The integrated lab-on-a-chip device proposed high-quality amplification results comparable to the conventional PCR. The repeatability of the results also demonstrates the device's reliability and simultaneous high-quality performance from different parts of the device. In some experiments (such as the ones in which the protocol involves a lower number of cycles), the bands obtained by on-chip PCR were even brighter than the conventional setup implying better amplification in the on-chip device.

Unlike other lab-on-a-chip devices, no microvalve or micropump is needed to push the mixture from the micromixer to the reaction chamber and hold it there during the thermocycling due to the special design of the device. Adding these components to the device would not only make the fabrication much more difficult, but also external devices would be needed to operate them. When fabrication becomes laborious, the chance of manufacturing a disposable device decreases. In most of these devices, the channels are washed upon PCR completion, even with dangerous materials such as piranha. This procedure is time-consuming and increases the chance of contamination and reactants degradation.

Nonetheless, the disposable feature of the proposed lab-on-a-chip device eliminates the run-to-run carryover contamination, while the easy-to-fabricate procedure makes it suitable for mass production.

6.2 Future work

The control unit of the proposed device is programmed to operate in the temperature range of common PCR protocols. In addition, the micromixer can handle different ratios of mixing between the master mix and the target virus. Therefore, the lab-on-a-chip device can be utilized to amplify other viruses or targets. It should be mentioned that preliminary tests were conducted with

cDNA as the target, and no degradation was observed. In addition, several microheaters can be fabricated on a single chip to increase the throughput of the system.

Compared to conventional PCR machines that consume 250W of power. Our microheater can operate in voltages under 9V with a power consumption of less than 1W. Therefore, it is possible to operate the whole system using commercial 12 V batteries. This modification will assist the portability of the device as well. In addition, optimizing the microheater in terms of power consumption and size is still possible, although considerable modifications have already been made to reach this pattern.

It is also possible to cut down on the mixing time by shortening the length of the mixer and making structural adjustments. Studies must be carried out to determine the best size, shapes, and angles for obstacles. These tests can be done by numerical simulation, but they must be validated through experiments as problems such as bubble formation will arise when working with pumps in a non-ideal environment. The simplicity and cost of the fabrication process must be taken into account to ensure that creating a disposable device is achievable. High-accuracy 3D printing with biocompatible materials might even enhance the chance of mass production of disposable parts of our device.

The main objective throughout designing the whole device was to increase the quality of amplification. We did not put extra effort into reducing the time of the process. However, several approaches can be implemented to speed up the process. For example, the PCR protocol can be modified. Reactant volume and dilution can be changed to reduce the number of cycles or dwell times and still produce bright bands. The sample volume can be reduced as well. Our preliminary tests suggested that a smaller sample size would result in a faster system.

Bibliography

[1] "COVID-19 Testing: What You Need to Know | CDC." https://www.cdc.gov/coronavirus/2019-ncov/symptoms-testing/testing.html (accessed Oct. 21, 2022).

[2] D. R. Reyes, D. Iossifidis, P. A. Auroux, and A. Manz, "Micro Total Analysis Systems. 1. Introduction, Theory, and Technology," *Anal Chem*, vol. 74, no. 12, pp. 2623–2636, Jun. 2002, doi: 10.1021/AC0202435.

[3] L. Chen, A. Manz, and P. J. R. Day, "Total nucleic acid analysis integrated on microfluidic devices," *Lab Chip*, vol. 7, no. 11, pp. 1413–1423, Oct. 2007, doi: 10.1039/B708362A.

[4] T. Satoh, S. Kouroki, Y. Kitamura, T. Ihara, K. Matsumura, and S. Iwase, "Detection of prostate-specific antigen in semen using DNA aptamers: an application of nucleic acid aptamers in forensic body fluid identification," *Analytical Methods*, vol. 12, no. 21, pp. 2703–2709, Jun. 2020, doi: 10.1039/D0AY00371A.

[5] B. Bruijns, R. Tiggelaar, and H. Gardeniers, "A Microfluidic Approach for Biosensing DNA within Forensics," *Applied Sciences*, vol. 10, no. 20, p. 7067, Oct. 2020, doi: 10.3390/app10207067.

[6] N. H. Ragland, E. L. Miedel, and R. W. Engelman, "PCR prevalence of murine opportunistic microbes and their mitigation by using vaporized hydrogen peroxide," *Journal of the American Association for Laboratory Animal Science*, vol. 58, no. 2, pp. 208–215, 2019, doi: 10.30802/AALAS-JAALAS-18-000112.

[7] K. Hamashima, Y. T. Soong, K. I. Matsunaga, M. Kimoto, and I. Hirao, "DNA Sequencing Method Including Unnatural Bases for DNA Aptamer Generation by Genetic

Alphabet Expansion," *ACS Synth Biol*, vol. 8, no. 6, pp. 1401–1410, Jun. 2019, doi: 10.1021/ACSSYNBIO.9B00087/SUPPL_FILE/SB9B00087_SI_001.PDF.

[8] K. Mullis, F. Faloona, S. Scharf, R. Saiki, G. Horn, and H. Erlich, "Specific Enzymatic Amplification of DNA In Vitro: The Polymerase Chain Reaction," *Cold Spring Harb Symp Quant Biol*, vol. 51, no. 1, pp. 263–273, Jan. 1986, doi: 10.1101/SQB.1986.051.01.032.

[9] "What are the differences between PCR, RT-PCR, qPCR, and RT-qPCR? - Enzo Life Sciences." https://www.enzolifesciences.com/science-center/technotes/2017/march/what-are-the-differences-between-pcr-rt-pcr-qpcr-and-rt-qpcr?/ (accessed Oct. 21, 2022).

[10] T. Vilkner, D. Janasek, and A. Manz, "Micro total analysis systems. Recent developments," *Anal Chem*, vol. 76, no. 12, pp. 3373–3386, Jun. 2004, doi: 10.1021/AC040063Q.

[11] P. A. Auroux, Y. Koc, A. DeMello, A. Manz, and P. J. R. Day, "Miniaturised nucleic acid analysis," *Lab Chip*, vol. 4, no. 6, pp. 534–546, 2004, doi: 10.1039/B408850F.

[12] "Nucleic Acids." https://www.genome.gov/genetics-glossary/Nucleic-Acids (accessed Oct. 21, 2022).

[13] K. Kadri and K. Kadri, "Polymerase Chain Reaction (PCR): Principle and Applications," *Synthetic Biology - New Interdisciplinary Science*, Jun. 2019, doi: 10.5772/INTECHOPEN.86491.

[14] "Fundamentals and Applications of Microfluidics, Third Edition - Nam-Trung Nguyen, Steven T. Wereley, Seyed Ali Mousavi Shaegh - Google Books." https://books.google.ca/books?hl=en&lr=&id=h3iFDwAAQBAJ&oi=fnd&pg=PP1&ots=e

92yNupUWX&sig=hXE_W90aNzzWiODQbkxzImrpT5U&redir_esc=y#v=onepage&q&f=false (accessed Oct. 05, 2022).

[15] "Polymerase Chain Reaction (PCR) Fact Sheet." https://www.genome.gov/about-genomics/fact-sheets/Polymerase-Chain-Reaction-Fact-Sheet (accessed Oct. 23, 2022).

[16] Y. Zhang and P. Ozdemir, "Microfluidic DNA amplification-A review," *Anal Chim Acta*, vol. 638, no. 2, pp. 115–125, 2009, doi: 10.1016/j.aca.2009.02.038.

[17] O. Geschke, H. Klank, and P. Telleman, "Microsystem Engineering of Lab-on-a-chip Devices".

[18] G. Whitesides, "The lab finally comes to the chip!," *Lab Chip*, vol. 14, no. 17, pp. 3125–3126, Jul. 2014, doi: 10.1039/C4LC90072C.

[19] T. H. Schulte, R. L. Bardell, and B. H. Weigl, "Microfluidic technologies in clinical diagnostics," *Clinica Chimica Acta*, vol. 321, no. 1–2, pp. 1–10, Jul. 2002, doi: 10.1016/S0009-8981(02)00093-1.

[20] C. Y. Lee and L. M. Fu, "Recent advances and applications of micromixers," *Sens Actuators B Chem*, vol. 259, pp. 677–702, 2018, doi: 10.1016/j.snb.2017.12.034.

[21] E. Samiei, M. Tabrizian, and M. Hoorfar, "A review of digital microfluidics as portable platforms for lab-on a-chip applications," *Lab Chip*, vol. 16, no. 13, pp. 2376–2396, Jun. 2016, doi: 10.1039/C6LC00387G.

[22] D. Cai, M. Xiao, P. Xu, Y. C. Xu, and W. Du, "An integrated microfluidic device utilizing dielectrophoresis and multiplex array PCR for point-of-care detection of pathogens," *Lab on a Chip - Miniaturisation for Chemistry and Biology*, vol. 14, no. 20, pp. 3917–3924, 2014, doi: 10.1039/c4lc00669k.

[23] G. v. Kaigala *et al.*, “An inexpensive and portable microchip-based platform for integrated RT–PCR and capillary electrophoresis,” *Analyst*, vol. 133, no. 3, pp. 331–338, Feb. 2008, doi: 10.1039/B714308G.

[24] F. Cui *et al.*, “Design and experiment of a PDMS-based PCR chip with reusable heater of optimized electrode,” *Microsystem Technologies*, vol. 23, no. 8, pp. 3069–3079, Aug. 2017, doi: 10.1007/s00542-016-3064-3.

[25] M. U. Kopp, A. J. de Mello, and A. Manz, “Chemical amplification: Continuous-flow PCR on a chip,” *Science (1979)*, vol. 280, no. 5366, pp. 1046–1048, May 1998, doi: 10.1126/SCIENCE.280.5366.1046.

[26] Y. Sun, Y. C. Kwok, and N. T. Nguyen, “A circular ferrofluid driven microchip for rapid polymerase chain reaction,” *Lab Chip*, vol. 7, no. 8, pp. 1012–1017, 2007, doi: 10.1039/b700575j.

[27] O. Frey, S. Bonneick, A. Hierlemann, and J. Lichtenberg, “Autonomous microfluidic multi-channel chip for real-time PCR with integrated liquid handling,” *Biomed Microdevices*, vol. 9, no. 5, pp. 711–718, 2007, doi: 10.1007/s10544-007-9080-4.

[28] N. Y. Lee, “A review on microscale polymerase chain reaction based methods in molecular diagnosis, and future prospects for the fabrication of fully integrated portable biomedical devices,” *Microchimica Acta*, vol. 185, no. 6, p. 285, Jun. 2018, doi: 10.1007/s00604-018-2791-9.

[29] M. B. Kulkarni and S. Goel, “Advances in continuous-flow based microfluidic PCR devices—a review,” *Engineering Research Express*, vol. 2, no. 4, p. 042001, Dec. 2020, doi: 10.1088/2631-8695/abd287.

[30] D. R. Almassian, L. M. Cockrell, and W. M. Nelson, “Portable nucleic acid thermocyclers,” *Chem Soc Rev*, vol. 42, no. 22, pp. 8769–8798, 2013, doi: 10.1039/c3cs60144g.

[31] H. C. Hunt and J. S. Wilkinson, “Optofluidic integration for microanalysis,” *Microfluid Nanofluidics*, vol. 4, no. 1–2, pp. 53–79, Jan. 2008, doi: 10.1007/S10404-007-0223-Y/FIGURES/21.

[32] Y. Liu *et al.*, “On-chip quantitative PCR using integrated real-time detection by capillary electrophoresis,” *Electrophoresis*, vol. 37, no. 3, pp. 545–552, Feb. 2016, doi: 10.1002/elps.201500298.

[33] E. T. Lagally, C. A. Emrich, and R. A. Mathies, “Fully integrated PCR-capillary electrophoresis microsystem for DNA analysis,” *Lab Chip*, vol. 1, no. 2, p. 102, 2001, doi: 10.1039/b109031n.

[34] L. Liu, W. Cao, J. Wu, W. Wen, D. C. Chang, and P. Sheng, “Design and integration of an all-in-one biomicrofluidic chip,” *Biomicrofluidics*, vol. 2, no. 3, p. 034103, Sep. 2008, doi: 10.1063/1.2966453.

[35] J. Jie *et al.*, “Portable and Battery-Powered PCR Device for DNA Amplification and Fluorescence Detection,” *Sensors*, vol. 20, no. 9, p. 2627, May 2020, doi: 10.3390/s20092627.

[36] J. H. Wang, L. Cheng, C. H. Wang, W. S. Ling, S. W. Wang, and G. bin Lee, “An integrated chip capable of performing sample pretreatment and nucleic acid amplification for HIV-1 detection,” *Biosens Bioelectron*, vol. 41, no. 1, pp. 484–491, 2013, doi: 10.1016/j.bios.2012.09.011.

[37] P. Zhu *et al.*, “Development and application of absolute quantitative detection by duplex chamber-based digital PCR of genetically modified maize events without pretreatment steps,” *Anal Chim Acta*, vol. 916, pp. 60–66, Apr. 2016, doi: 10.1016/J.ACA.2016.02.020.

[38] B. Miao *et al.*, “Centrifugal Microfluidic System for Nucleic Acid Amplification and Detection,” *Sensors 2015, Vol. 15, Pages 27954-27968*, vol. 15, no. 11, pp. 27954–27968, Nov. 2015, doi: 10.3390/S151127954.

[39] A. A. Morley, “Digital PCR: A brief history,” *Biomol Detect Quantif*, vol. 1, no. 1, pp. 1–2, 2014, doi: 10.1016/J.BDQ.2014.06.001.

[40] C.-S. Liao, “Miniature RT-PCR system for diagnosis of RNA-based viruses,” *Nucleic Acids Res*, vol. 33, no. 18, pp. e156–e156, Oct. 2005, doi: 10.1093/nar/gni157.

[41] C. Fang, F. Ji, Z. Shu, and D. Gao, “Determination of the temperature-dependent cell membrane permeabilities using microfluidics with integrated flow and temperature control,” *Lab Chip*, vol. 17, no. 5, pp. 951–960, 2017, doi: 10.1039/C6LC01523A.

[42] E. A. Oblath, W. H. Henley, J. P. Alarie, and J. M. Ramsey, “A microfluidic chip integrating DNA extraction and real-time PCR for the detection of bacteria in saliva,” *Lab Chip*, vol. 13, no. 7, p. 1325, 2013, doi: 10.1039/c3lc40961a.

[43] K.-Y. Lien, W.-C. Lee, H.-Y. Lei, and G.-B. Lee, “Integrated reverse transcription polymerase chain reaction systems for virus detection,” *Biosens Bioelectron*, vol. 22, no. 8, pp. 1739–1748, Mar. 2007, doi: 10.1016/j.bios.2006.08.010.

[44] K. Shen, X. Chen, M. Guo, and J. Cheng, “A microchip-based PCR device using flexible printed circuit technology,” *Sens Actuators B Chem*, vol. 105, no. 2, pp. 251–258, Mar. 2005, doi: 10.1016/j.snb.2004.05.069.

[45] P. K. Guha *et al.*, “Novel design and characterisation of SOI CMOS micro-hotplates for high temperature gas sensors,” *Sens Actuators B Chem*, vol. 127, no. 1, pp. 260–266, Oct. 2007, doi: 10.1016/J.SNB.2007.07.047.

[46] H. Nagai, Y. Murakami, K. Yokoyama, and E. Tamiya, “High-throughput PCR in silicon based microchamber array,” *Biosens Bioelectron*, vol. 16, no. 9–12, pp. 1015–1019, 2001, doi: 10.1016/S0956-5663(01)00248-2.

[47] K. Hu, Z. Chen, and J. Huang, “Research on temperature measuring positions selection and verification for Polymerase Chain Reaction instruments,” *Proceedings - 2011 4th International Conference on Biomedical Engineering and Informatics, BMEI 2011*, vol. 3, pp. 1165–1169, 2011, doi: 10.1109/BMEI.2011.6098553.

[48] M. G. Roper, C. J. Easley, L. A. Legendre, J. A. C. Humphrey, and J. P. Landers, “Infrared temperature control system for a completely noncontact polymerase chain reaction in microfluidic chips,” *Anal Chem*, vol. 79, no. 4, pp. 1294–1300, Feb. 2007, doi: 10.1021/AC0613277/SUPPL_FILE/AC0613277SI20060809_114422.PDF.

[49] N. Pak, D. C. Saunders, C. R. Phaneuf, and C. R. Forest, “Plug-and-play, infrared, laser-mediated PCR in a microfluidic chip,” *Biomed Microdevices*, vol. 14, no. 2, pp. 427–433, Apr. 2012, doi: 10.1007/S10544-011-9619-2/FIGURES/5.

[50] N. Beyor, L. Yi, S. S. Tae, and R. A. Mathies, “Integrated Capture, Concentration, Polymerase Chain Reaction, and Capillary Electrophoretic Analysis of Pathogens on a Chip,” *Anal Chem*, vol. 81, no. 9, pp. 3523–3528, May 2009, doi: 10.1021/AC900060R.

[51] C. Zhang and D. Xing, “Miniaturized PCR chips for nucleic acid amplification and analysis: latest advances and future trends,” *Nucleic Acids Res*, vol. 35, no. 13, pp. 4223–4237, Jul. 2007, doi: 10.1093/NAR/GKM389.

[52] C. D. Ahrberg, B. R. Ilic, A. Manz, and P. Neužil, “Handheld real-time PCR device,” *Lab Chip*, vol. 16, no. 3, pp. 586–592, 2016, doi: 10.1039/c5lc01415h.

[53] T.-M. Hsieh, C.-H. Luo, F.-C. Huang, J.-H. Wang, L.-J. Chien, and G.-B. Lee, “Enhancement of thermal uniformity for a microthermal cycler and its application for polymerase chain reaction☆,” *Sens Actuators B Chem*, vol. 130, no. 2, pp. 848–856, Mar. 2008, doi: 10.1016/j.snb.2007.10.063.

[54] J. El-Ali, I. R. Perch-Nielsen, C. R. Poulsen, D. D. Bang, P. Telleman, and A. Wolff, “Simulation and experimental validation of a SU-8 based PCR thermocycler chip with integrated heaters and temperature sensor,” *Sens Actuators A Phys*, vol. 110, no. 1–3, pp. 3–10, Feb. 2004, doi: 10.1016/j.sna.2003.09.022.

[55] H.-W. Veltkamp, F. Akegawa Monteiro, R. Sanders, R. Wiegerink, and J. Lötters, “Disposable DNA Amplification Chips with Integrated Low-Cost Heaters †,” *Micromachines (Basel)*, vol. 11, no. 3, p. 238, Feb. 2020, doi: 10.3390/mi11030238.

[56] J. Martinez-Quijada *et al.*, “Deterministic Design of Thin-Film Heaters for Precise Spatial Temperature Control in Lab-on-Chip Systems,” *Journal of Microelectromechanical Systems*, vol. 25, no. 3, pp. 508–516, Jun. 2016, doi: 10.1109/JMEMS.2016.2536561.

[57] Z. Y. Wu, K. Chen, B. Y. Qu, X. X. Tian, X. J. Wang, and F. Fang, “A thermostat chip of indium tin oxide glass substrate for static polymerase chain reaction and in situ real time fluorescence monitoring,” *Anal Chim Acta*, vol. 610, no. 1, pp. 89–96, Mar. 2008, doi: 10.1016/j.aca.2007.12.044.

[58] T.-M. Hsieh, C.-H. Luo, J.-H. Wang, J.-L. Lin, K.-Y. Lien, and G.-B. Lee, “A two-dimensional, self-compensated, microthermal cycler for one-step reverse transcription

polymerase chain reaction applications," *Microfluid Nanofluidics*, vol. 6, no. 6, pp. 797–809, Jun. 2009, doi: 10.1007/s10404-008-0353-x.

[59] J. Wu, R. Kodzius, K. Xiao, J. Qin, and W. Wen, "Fast detection of genetic information by an optimized PCR in an interchangeable chip," *Biomed Microdevices*, vol. 14, no. 1, pp. 179–186, Feb. 2012, doi: 10.1007/s10544-011-9595-6.

[60] F.-C. Huang, C.-S. Liao, and G.-B. Lee, "An integrated microfluidic chip for DNA/RNA amplification, electrophoresis separation and on-line optical detection," *Electrophoresis*, vol. 27, no. 16, pp. 3297–3305, Aug. 2006, doi: 10.1002/elps.200600458.

[61] D. Resnik, D. Vrtačnik, M. Možek, B. Pečar, and S. Amon, "Experimental study of heat-treated thin film Ti/Pt heater and temperature sensor properties on a Si microfluidic platform," *Journal of Micromechanics and Microengineering*, vol. 21, no. 2, p. 025025, Jan. 2011, doi: 10.1088/0960-1317/21/2/025025.

[62] N. Beyor, L. Yi, S. S. Tae, and R. A. Mathies, "Integrated Capture, Concentration, PCR, and Capillary Electrophoretic Analysis of Pathogens on a Chip," *Anal Chem*, vol. 81, no. 9, p. 3523, May 2009, doi: 10.1021/AC900060R.

[63] P. Bhattacharyya, "Technological journey towards reliable microheater development for MEMS gas sensors: a review," *IEEE Transactions on Device and Materials Reliability*, vol. 14, no. 2, pp. 589–599, 2014, doi: 10.1109/TDMR.2014.2311801.

[64] K. Sun, A. Yamaguchi, Y. Ishida, S. Matsuo, and H. Misawa, "A heater-integrated transparent microchannel chip for continuous-flow PCR," *Sens Actuators B Chem*, vol. 84, no. 2–3, pp. 283–289, May 2002, doi: 10.1016/S0925-4005(02)00016-3.

[65] D. J. Sadler, R. Changrani, P. Roberts, C. F. Chou, and F. Zenhausern, "Thermal management of bioMEMS: Temperature control for ceramic-based PCR and DNA

detection devices," *IEEE Transactions on Components and Packaging Technologies*, vol. 26, no. 2, pp. 309–316, Jun. 2003, doi: 10.1109/TCAPT.2003.815093.

[66] C. T. Culbertson, T. G. Mickleburgh, S. A. Stewart-James, K. A. Sellens, and M. Pressnall, "Micro Total Analysis Systems: Fundamental Advances and Biological Applications," *Anal Chem*, vol. 86, no. 1, p. 95, Jan. 2014, doi: 10.1021/AC403688G.

[67] V. Rudyak and A. Minakov, "Modeling and optimization of Y-type micromixers," *Micromachines (Basel)*, vol. 5, no. 4, pp. 886–912, 2014, doi: 10.3390/mi5040886.

[68] "Micromixers: Fundamentals, Design and Fabrication - Nam-Trung Nguyen - Google Books." https://books.google.ca/books?hl=en&lr=&id=BHB0fBQuifkC&oi=fnd&pg=PP1&ots=cSbyS4vvHH&sig=cs_BThlrWYhyWgWSgT5OtYvAbcA&redir_esc=y#v=onepage&q&f=false (accessed Oct. 05, 2022).

[69] G. S. Jeong, S. Chung, C. B. Kim, and S. H. Lee, "Applications of micromixing technology," *Analyst*, vol. 135, no. 3, pp. 460–473, 2010, doi: 10.1039/b921430e.

[70] E. le Rouzic, "Contamination-pipetting: relative efficiency of filter tips compared to Microman® positive displacement pipette," *Nature Methods 2006 3:6*, vol. 3, no. 6, pp. III–IV, May 2006, doi: 10.1038/nmeth887.

[71] K. Lyman, D. Fisher, Y. Han, and D. M. Chetkovich, "A novel method for reducing human pipetting errors," vol. 6, no. 6, pp. 36–40, 2015, doi: 10.5897/JMLD2015.0110.

[72] "(PDF) Assessment of Pipetting Errors and its Contribution in Analytical Performance in A Tertyiary Care Hospital | ResearchGate." https://www.researchgate.net/publication/303994774_Assessment_of_Pipetting_Errors_an

d_its_Contribution_in_Analytical_Performance_in_A_Tertyiary_Care_Hospital (accessed Oct. 03, 2022).

[73] H. van Phan, M. B. Coşkun, M. Şeşen, G. Pandraud, A. Neild, and T. Alan, "Vibrating membrane with discontinuities for rapid and efficient microfluidic mixing," *Lab Chip*, vol. 15, no. 21, pp. 4206–4216, 2015, doi: 10.1039/C5LC00836K.

[74] V. Hessel, H. Löwe, and F. Schönfeld, "Micromixers—a review on passive and active mixing principles," *Chem Eng Sci*, vol. 60, no. 8–9, pp. 2479–2501, Apr. 2005, doi: 10.1016/J.CES.2004.11.033.

[75] M. Bayareh, M. N. Ashani, and A. Usefian, "Active and passive micromixers: A comprehensive review," *Chemical Engineering and Processing - Process Intensification*, vol. 147, no. December 2019, p. 107771, Jan. 2020, doi: 10.1016/j.cep.2019.107771.

[76] G. Cai, L. Xue, H. Zhang, and J. Lin, "A Review on Micromixers," *Micromachines (Basel)*, vol. 8, no. 9, p. 274, Sep. 2017, doi: 10.3390/mi8090274.

[77] X. Niu and Y. K. Lee, "Efficient spatial-temporal chaotic mixing in microchannels," *Journal of Micromechanics and Microengineering*, vol. 13, no. 3, p. 454, Apr. 2003, doi: 10.1088/0960-1317/13/3/316.

[78] T. D. Luong, V. N. Phan, and N. T. Nguyen, "High-throughput micromixers based on acoustic streaming induced by surface acoustic wave," *Microfluid Nanofluidics*, vol. 10, no. 3, pp. 619–625, Mar. 2011, doi: 10.1007/S10404-010-0694-0/FIGURES/8.

[79] D. Nouri, A. Zabihi-Hesari, and M. Passandideh-Fard, "Rapid mixing in micromixers using magnetic field," *Sens Actuators A Phys*, vol. 255, pp. 79–86, Mar. 2017, doi: 10.1016/J.SNA.2017.01.005.

[80] J. J. Huang, Y. J. Lo, C. M. Hsieh, U. Lei, C. I. Li, and C. W. Huang, “An electro-thermal micro mixer,” *NEMS 2011 - 6th IEEE International Conference on Nano/Micro Engineered and Molecular Systems*, pp. 919–922, 2011, doi: 10.1109/NEMS.2011.6017503.

[81] L. Capretto, W. Cheng, M. Hill, and X. Zhang, “Micromixing within microfluidic devices,” *Top Curr Chem*, vol. 304, pp. 27–68, 2011, doi: 10.1007/128_2011_150/FIGURES/20_150.

[82] W. Raza, S. Hossain, and K.-Y. Kim, “A Review of Passive Micromixers with a Comparative Analysis,” *Micromachines (Basel)*, vol. 11, no. 5, p. 455, Apr. 2020, doi: 10.3390/mi11050455.

[83] R. A. Vijayendran, K. M. Motsegood, D. J. Beebe, and D. E. Leckband, “Evaluation of a three-dimensional micromixer in a surface-based biosensor,” *Langmuir*, vol. 19, no. 5, pp. 1824–1828, Mar. 2003, doi: 10.1021/LA0262250/ASSET/IMAGES/LARGE/LA0262250F00005.JPEG.

[84] R. H. Liu *et al.*, “Passive mixing in a three-dimensional serpentine microchannel,” *Journal of Microelectromechanical Systems*, vol. 9, no. 2, pp. 190–197, Jun. 2000, doi: 10.1109/84.846699.

[85] V. Viktorov, M. R. Mahmud, and C. Visconte, “Numerical study of fluid mixing at different inlet flow-rate ratios in Tear-drop and Chain micromixers compared to a new H-C passive micromixer,” *http://www.tandfonline.com/action/authorSubmission?journalCode=tcfm20&page=instructions*, vol. 10, no. 1, pp. 183–193, Jan. 2016, doi: 10.1080/19942060.2016.1140075.

[86] M. Nimafar, V. Viktorov, and M. Martinelli, “Experimental comparative mixing performance of passive micromixers with H-shaped sub-channels,” *Chem Eng Sci*, vol. 76, pp. 37–44, Jul. 2012, doi: 10.1016/J.CES.2012.03.036.

[87] M. Rafeie, M. Welleweerd, A. Hassanzadeh-Barforoushi, M. Asadnia, W. Olthuis, and M. E. Warkiani, “An easily fabricated three-dimensional threaded lemniscate-shaped micromixer for a wide range of flow rates,” *Biomicrofluidics*, vol. 11, no. 1, p. 014108, Jan. 2017, doi: 10.1063/1.4974904.

[88] A. S. Yang *et al.*, “A high-performance micromixer using three-dimensional Tesla structures for bio-applications,” *Chemical Engineering Journal*, vol. 263, pp. 444–451, Mar. 2015, doi: 10.1016/J.CEJ.2014.11.034.

[89] W. Raza, S. Hossain, and K. Y. Kim, “A review of passive micromixers with a comparative analysis,” *Micromachines (Basel)*, vol. 11, no. 5, 2020, doi: 10.3390/MI11050455.

[90] A. Afzal and K. Y. Kim, “Convergent–divergent micromixer coupled with pulsatile flow,” *Sens Actuators B Chem*, vol. 211, pp. 198–205, May 2015, doi: 10.1016/J.SNB.2015.01.062.

[91] A. P. Sudarsan and V. M. Ugaz, “Fluid mixing in planar spiral microchannels,” *Lab Chip*, vol. 6, no. 1, pp. 74–82, Dec. 2006, doi: 10.1039/B511524H.

[92] L. Wang, S. Ma, X. Wang, H. Bi, and X. Han, “Mixing enhancement of a passive microfluidic mixer containing triangle baffles,” *Asia-Pacific Journal of Chemical Engineering*, vol. 9, no. 6, pp. 877–885, Nov. 2014, doi: 10.1002/apj.1837.

[93] X. Li, H. Chang, X. Liu, F. Ye, and W. Yuan, “A 3-D Overbridge-Shaped Micromixer for Fast Mixing Over a Wide Range of Reynolds Numbers,” *Journal of*

Microelectromechanical Systems, vol. 24, no. 5, pp. 1391–1399, Oct. 2015, doi: 10.1109/JMEMS.2015.2403472.

[94] N.-T. Nguyen and Z. Wu, "Micromixers—a review," *Journal of Micromechanics and Microengineering*, vol. 15, no. 2, pp. R1–R16, Feb. 2005, doi: 10.1088/0960-1317/15/2/R01.

[95] Y. Zhang, Y. Hu, and H. Wu, "Design and simulation of passive micromixers based on capillary," *Microfluid Nanofluidics*, vol. 13, no. 5, pp. 809–818, Nov. 2012, doi: 10.1007/S10404-012-1002-Y/FIGURES/12.

[96] V. Viktorov, M. R. Mahmud, and C. Visconte, "Numerical study of fluid mixing at different inlet flow-rate ratios in Tear-drop and Chain micromixers compared to a new H-C passive micromixer," *Engineering Applications of Computational Fluid Mechanics*, vol. 10, no. 1, pp. 183–193, 2016, doi: 10.1080/19942060.2016.1140075.

[97] R. R. Gidde and P. M. Pawar, "Flow Feature Analysis of T-Junction Wavy Micromixer for Mixing Application," *International Journal of Chemical Reactor Engineering*, vol. 17, no. 9, pp. 1–15, 2019, doi: 10.1515/ijcre-2018-0306.

[98] K. Karthikeyan and L. Sujatha, "Study of Permissible Flow Rate and Mixing Efficiency of the Micromixer Devices," *International Journal of Chemical Reactor Engineering*, vol. 17, no. 1, pp. 1–15, Jan. 2019, doi: 10.1515/ijcre-2018-0047.

[99] A. Hashmi and J. Xu, "On the Quantification of Mixing in Microfluidics," *J Lab Autom*, vol. 19, no. 5, pp. 488–491, Oct. 2014, doi: 10.1177/2211068214540156/ASSET/IMAGES/LARGE/10.1177_2211068214540156-FIG2.JPEG.

[100] R. Syms, “Rapid evaporation-driven chemical pre-concentration and separation on paper,” *Biomicrofluidics*, vol. 11, no. 4, Jul. 2017, doi: 10.1063/1.4989627.